



CHALMERS
UNIVERSITY OF TECHNOLOGY

Marine Fuel Regulations and Engine Emissions: Impacts on Physicochemical Properties, Cloud Activity and Emission Factors

Downloaded from: <https://research.chalmers.se>, 2026-04-04 16:01 UTC

Citation for the original published paper (version of record):

Santos, L., Salo, K., Kong, X. et al (2024). Marine Fuel Regulations and Engine Emissions: Impacts on Physicochemical Properties, Cloud Activity and Emission Factors. *Journal of Geophysical Research: Atmospheres*, 129(5).
<http://dx.doi.org/10.1029/2023JD040389>

N.B. When citing this work, cite the original published paper.

Special Section:

Emerging air pollution: emissions, chemistry, and health and climate effects

Key Points:

- Low sulfur content fuels can reduce emissions of ultrafine particulate matter significantly
- Exhaust wet scrubbing can lead to shifts in particle size distributions and reduce soot emissions
- Usage of low sulfur content fuels or exhaust wet scrubbing have opposing effects on CCN activity of ship exhaust particles

Supporting Information:

Supporting Information may be found in the online version of this article.

Correspondence to:

L. F. E. D. Santos and E. S. Thomson,
luis.santos@cmb.gu.se;
erik.thomson@chem.gu.se

Citation:

Santos, L. F. E. D., Salo, K., Kong, X., Hartmann, M., Sjöblom, J., & Thomson, E. S. (2024). Marine fuel regulations and engine emissions: Impacts on physicochemical properties, cloud activity and emission factors. *Journal of Geophysical Research: Atmospheres*, 129, e2023JD040389. <https://doi.org/10.1029/2023JD040389>

Received 15 NOV 2023

Accepted 8 FEB 2024

Author Contributions:

Conceptualization: L. F. E. D. Santos, K. Salo, X. Kong, J. Sjöblom, E. S. Thomson

Data curation: L. F. E. D. Santos, K. Salo, X. Kong, M. Hartmann

Formal analysis: L. F. E. D. Santos, X. Kong, M. Hartmann

© 2024. The Authors.

This is an open access article under the terms of the [Creative Commons Attribution-NonCommercial-NoDerivs License](https://creativecommons.org/licenses/by/4.0/), which permits use and distribution in any medium, provided the original work is properly cited, the use is non-commercial and no modifications or adaptations are made.

Marine Fuel Regulations and Engine Emissions: Impacts on Physicochemical Properties, Cloud Activity and Emission Factors

L. F. E. D. Santos¹ , K. Salo², X. Kong¹ , M. Hartmann^{1,3} , J. Sjöblom⁴, and E. S. Thomson¹ 

¹Department of Chemistry and Molecular Biology, Atmospheric Science, University of Gothenburg, Gothenburg, Sweden, ²Department of Mechanics and Maritime Sciences, Maritime Studies, Chalmers University of Technology, Gothenburg, Sweden, ³Now at Department for Atmospheric Microphysics, Leibniz Institute for Tropospheric Research, Leipzig, Germany, ⁴Department of Mechanics and Maritime Sciences, Combustion and Propulsion Systems, Chalmers University of Technology, Gothenburg, Sweden

Abstract Marine regulations aim to reduce sulfur and nitrogen exhaust emissions from maritime shipping. Here, two compliance pathways for reducing sulfur dioxide emissions, fuel sulfur content reduction and exhaust wet scrubbing, are studied for their effects on physicochemical properties and cloud forming abilities of engine exhaust particles. A test-bed diesel engine was utilized to study fresh exhaust emissions from combustion of non-compliant, high sulfur content fuel with (WS) and without (HiS) the usage of a wet scrubber as well as a regulatory compliant, low sulfur content fuel (LoS). Particle number emissions are decreased by $\approx 99\%$ when switching to LoS due to absence of 20–30 nm sulfate rich particles. While number emissions for WS are also decreased, a shift in the sulfate mode toward larger sizes was found to increase particle mass emission factors by at least 31%. Changes in the mixing state induced by the compliance measures are reflected in the hygroscopicity of the exhaust particles. Fuel sulfur reduction decreased cloud condensation nuclei emissions by at least 97% due to emissions of primarily hydrophobic soot particles. Wet scrubbing increased those emissions, mainly driven by changes in particle size distributions. Our results indicate that both compliance alternatives have no obvious impact on the ice forming abilities of 200 nm exhaust particles. These detailed results are relevant for atmospheric processes and might be useful input parameters for cloud-resolving models to investigate ship aerosol-cloud interactions and to quantify the impact of shipping on radiative budgets from local to global scales.

Plain Language Summary We investigate how two pathways to comply with international regulations, aiming to reduce emissions of atmospheric pollutants from ships, alter properties of exhaust particles. Both investigated compliance measures (i.e., combustion of cleaner, low sulfur content fuels and aftertreatment of exhaust from a high sulfur content fuel via wet scrubbing) have substantial impacts on the chemical and physical properties of these particles. We find that, while both alternatives reduce the total number of emitted particles substantially, the effect on emissions of cloud forming particles is path dependent. While fuel sulfur content reduction decreased the number of cloud forming particles by about 97%, wet scrubbing led to a strong increase in emissions, suggesting that the measures can have substantial and opposing impacts on local cloud formation and evolution.

1. Introduction

Maritime shipping is a significant source of atmospheric pollutants (NO_x and SO_2), greenhouse gases (CO_2), and exhaust particles in the form of soot and sulfate that can have negative impacts on human health and ecosystems. Exhaust particles from ships have been found to impact human health along coasts and in areas close to major shipping lanes due to high ultrafine particle numbers and the chemical compositions of these particles (Corbett et al., 2007; Liu et al., 2016). Ship exhaust particles generally consist of carbonaceous matter, often in the form of soot or other organics, inorganic species, such as sulfate, ash and can also contain different metals minerals originating from the fuels or lubricating oils (Eichler et al., 2017; Moldanová et al., 2013; Popovicheva et al., 2009). Given the range of fuel types and engines used in the shipping sector, the relative contributions between constituents can vary significantly.

To address air pollution from ship exhaust particles the International Maritime Organization (IMO) has been implementing international regulations, which target emission reductions of sulfur oxides (SO_x) and also,

Funding acquisition: K. Salo, X. Kong, J. Sjöblom, E. S. Thomson
Investigation: L. F. E. D. Santos, K. Salo, X. Kong, M. Hartmann, J. Sjöblom, E. S. Thomson
Methodology: L. F. E. D. Santos, K. Salo, X. Kong, M. Hartmann, J. Sjöblom, E. S. Thomson
Project administration: L. F. E. D. Santos, K. Salo, J. Sjöblom, E. S. Thomson
Resources: K. Salo, J. Sjöblom, E. S. Thomson
Software: M. Hartmann
Supervision: L. F. E. D. Santos, K. Salo, X. Kong, J. Sjöblom, E. S. Thomson
Validation: L. F. E. D. Santos, K. Salo, X. Kong, M. Hartmann, J. Sjöblom, E. S. Thomson
Visualization: L. F. E. D. Santos
Writing – original draft: L. F. E. D. Santos, E. S. Thomson
Writing – review & editing: L. F. E. D. Santos, K. Salo, X. Kong, M. Hartmann, J. Sjöblom, E. S. Thomson

indirectly particulate matter from ships. The regulations mandate ship owners emit less SO₂. Operators can achieve this by transitioning to higher grade marine fuels with lower fuel sulfur content (FSC) or by installing exhaust abatement systems, such as wet scrubbers, which are primarily designed to remove SO₂ from the exhaust. In the absence of SO₂ removal systems, the FSC of marine fuels is limited to 0.5% by mass (hereafter abbreviated by %). In sulfur emission control areas (SECA), which include the Baltic and North Sea area among others, regulations are stricter and the FSC of marine fuels may not exceed 0.1% (IMO, 2008).

Recent studies show that particulate emissions have coincidentally been reduced following the implementation of both, a 2015 0.1% SECA limit and a global 2020 0.5% FSC cap (Anastasopoulos et al., 2021; Seppälä et al., 2021; Wu et al., 2020; Yu et al., 2020, 2023). This complimentary particle reduction is likely caused by shifts toward higher grade residual fuel oils and distillate fuels or due to blending of fuels to meet FSC compliance levels. Anastasopoulos et al. (2021), for example, investigated effects after implementation of the aforementioned restrictions on particulate matter emissions along coastal areas in North America and observed large reductions in SO₂ and particulate matter concentrations (up to 83% and 37% respectively). Moreover, a ship plume intercept study over the Baltic Sea found ambient particle concentrations to be reduced by up to 32% after implementation of the 0.1% SECA FSC restrictions (Seppälä et al., 2021). Similar reductions of particulate matter emissions were also observed for ships utilizing fuels with FSCs below 0.5% (Yu et al., 2020, 2023). While one study showed that ships at berth emitted on average 56% less particles, restrictions were also found to affect the emission characteristics of volatile organic compounds and the potential for secondary aerosol and ozone formation to be significantly increased, which has implications for local air quality (Wu et al., 2020). Despite implementations of stricter FSC restrictions and a resulting reduction in emission of various air pollutants, ship related emissions of particulate matter and NO_x can still be a major burden on ambient air quality in major port areas (Zhai et al., 2023). While a clear trend for particle number concentration reductions is seen, transitions toward lower FSC fuels have also been found to reduce the potential of exhaust particles to form liquid droplets at atmospherically relevant supersaturations. This decrease of cloud condensation nuclei (CCN) emissions is due to reduced emissions of more hygroscopic particles and shifts toward emissions of generally smaller particles, which have higher droplet activation thresholds (Santos et al., 2023; Yu et al., 2020, 2023).

While wet scrubbing has been found to reliably decrease ship exhaust SO₂ emissions to IMO compliant levels, recent studies on exhaust particle removal efficiencies show varying results. Fridell and Salo (2016) found particle number concentrations to be reduced by approximately 92% and Winnes et al. (2020) found significant reductions in total number emissions but not in the solid fraction of exhaust particles. Conversely, other studies report only minor reductions in total particle number concentrations (Lehtoranta et al., 2019) or find only particles above 1 μm to be efficiently removed (Zhou et al., 2017). Similarly, Yang et al. (2021) found particulate matter below 2.5 μm to be reduced by ≈10% but found the level of sulfate particles to be hardly affected. More recent wet scrubber studies investigated the implementation of a wet electrostatic precipitator (WESP) after a scrubber and found that up to 98% of the exhaust particles were removed (Järvinen et al., 2023; Jeong et al., 2023). Moreover, exhaust particle wet scrubbing has been found to affect the composition and mixing state of exhaust particles (Lieke et al., 2013; Santos et al., 2023), which can alter their roles in atmospheric processes, for example, by facilitating liquid droplet formation (Santos et al., 2023). The introduction of exhaust wet scrubbing in the shipping sector has also gained attention for its potential hazardous impacts on the marine environment and its lifeforms. Studies have found that open-loop scrubbing leads to concentrated emissions of metals and PAHs to the water and can also lead to emissions of new contaminants, like chromium (Lunde Hermansson et al., 2021; Ytreberg et al., 2022).

Maritime shipping emissions and ship track observations provide a good opportunity to study the role of anthropogenic emissions on the climate system. For instance, the recent introduction of the global 0.5% FSC limit can be used to investigate the impact of reduced SO_x emissions from ships on cloud formation and properties, and to better quantify radiative forcing. Yuan et al. (2022) found that the 2020 FSC cap led to a decrease in ship track frequency and subsequently a reduction of climate cooling from emitted aerosol particles. While Gryspeerdt et al. (2019) observed large reductions in ship track numbers between 2014 and 2015 and highlight sulfate as the key component in ship track formation, they also point out difficulties in detecting ship tracks due to uncertainties in background cloud states, which can lead to an underestimate of the actual impact from shipping. Similarly, Manshausen et al. (2022) found that ships can form “invisible” tracks, which may not be directly visible but their aerosol emissions can still alter cloud properties. These uncertainties in quantifying climate impacts from maritime shipping have also been highlighted by Watson-Parris et al. (2022), which found that an 80% reduction

Table 1
Fuel Properties

	HiS	LoS
Density at 15°C (kg/m ³)	865.7	837.3
Heat of combustion (MJ/kg)		
Gross heat of combustion	45.10	45.73
Sulfur content (mass %)	0.63	0.041
Aromatic content (mass %)		
Total aromatics	32.5	22.3
Mono-aromatics	20.8	18.3
Di-aromatics	10.2	3.5
Tri + aromatics	1.5	0.5
Additive and wear metals (mg/kg)		
B	0.17	<0.1
K	0.29	0.60
Al, Ca, Cr, Cu, Fe, Pb	<0.1	<0.1
Ni, Na, V, P, Sn, Zn, Zi	<0.1	<0.1

Note. The cetane numbers for the tested fuels were within specifications for the engine. Fuel analysis was conducted by Saybolt Sweden in Gothenburg.

2.2. Engine, Fuels and Laboratory Wet-Scrubber

Engine experiments were performed at Chalmers University of Technology in Sweden using a Volvo D13K540 Euro 6 common rail, four-stroke diesel engine equipped with six cylinders, a bore of 131 mm and a stroke of 158 mm. The engine's on-road aftertreatment system was removed prior to experiments. The engine was operated at 1,200 rpm during experiments, resulting in a maximum torque of 2,600 Nm and maximum power output of 349 kW. To study the engine load dependence of particle exhaust emissions, measurements were performed at engine load points of 25% (≈ 85 kW), 50% (≈ 168 kW) and 70% (≈ 245 kW). Different engine loads also serve to mimic different operational conditions of ships and therefore, allow particle exhaust emissions during such operations to be studied. For example, engine loads of 50% and 70% typically represent ships at different cruising conditions, whereas 25% load reflects maneuvering situations, for example, in port areas. The tested engine loads were determined from the ratios between measured and maximum torque at 1,200 rpm.

To investigate the effects of FSC on physicochemical properties and cloud activity of exhaust particles, two fuels were used during the experiments. Here, the baseline case (no compliance) is a marine distillate fuel with a FSC of 0.63% (HiS) exceeding the global FSC limit of 0.5%. Note that HiS fuel is a distillate fuel and thus, has a lower density and viscosity compared to residual fuel oils, which are also commonly used in maritime shipping. The compliant, low FSC fuel used during experiments was marine gas oil (MGO) which had a

FSC of 0.041% and is commonly used in the shipping sector. This case will be referred to as LoS. Fuel characteristics details are found in Table 1.

Since measurements outlined in this study are complicated and expensive to perform on-board ships during operation, a lab-scale engine set-up was chosen. This engine and similar setups have been used to test abatement technologies and different marine fuels and their effect on the exhaust gas composition (Anderson et al., 2015; Flagiello et al., 2021; Zetterdahl et al., 2017). It has been demonstrated to be a representative and cost-effective method for these types of studies. Results from such tests can be extrapolated to estimate the performance of larger engines. However, it is important to note that scale-dependent phenomena may not be perfectly represented by smaller engines.

A custom-built, laboratory-scale wet-scrubber engineered at Chalmers University of Technology was used during specified experiments to reduce SO_x emissions from HiS combustion and to study the effects of wet scrubbing on exhaust particles. The unit consists of a horizontal, cylindrical 50 cm stainless steel tank with an inner diameter of 40 cm. In total, seven nozzles, controlled by a pressure pump, are used to spray a fine mist of seawater into the exhaust gas. Three perforated demister plates are mounted inside the scrubber to enhance droplet removal from the exhaust gas before it leaves through the outlet. A more detailed description of the wet-scrubber can be found in Santos et al. (2022). In addition, lattice-structured packing material was placed between the demister plates to increase surface interaction between exhaust gas and packing material to enhance the particle and droplet removal efficiency. Seawater used during the experiments was obtained from University of Gothenburg's Kristineberg Center for Marine Research and Innovation located on the Gullmar fjord in western Sweden (58°14'59.7"N 11°26'41.3"E). While surface water in the Gullmar fjord is characterized by water from the Baltic Sea and Kattegat/Skaggeak, water at greater depths is influenced by high saline bottom water from the North Sea. In this study, we used exclusively the facility's deep water system with an intake depth of 32 m and thus, the water possesses a relatively high and stable salinity. Measurement data shows that the salinity of the deep water is typically ≈ 33 PSU (Kristineberg Center Homepage, 2024).

2.3. Gas and Aerosol Instrumentation

Raw exhaust gas was diluted using a 2-stage dilution system (FPS-4000, Dekati Ltd., Finland) consisting of a temperature-controlled porous tube diluter as the first stage and an ejector diluter as the second stage. A single-beam NDIR analyzer (Model ZRE, Fuji Electric Co., Ltd., Japan) was used to measure relevant gaseous

compounds including O₂, CO₂, CO, NO_x and SO₂ in the raw exhaust. The CO₂ concentration after the dilution system was measured with a Fuji ZPG CO and CO₂ analyzer (Fuji Electric Co., Ltd., Japan) and corrected for background CO₂ concentrations measured before engine start up. The ratios between CO₂ concentrations in the raw and diluted exhaust gas were used to calculate dilution ratios. A dilution system was used because high particle concentrations in the raw exhaust gas would have saturated most of the aerosol measurement instrumentation.

The diluted sample aerosol was dried using silica gel diffusion dryers before being passed to the particle analysis instrumentation. Particle size distributions (PSD) were measured using a scanning mobility particle sizer (SMPS; Electrostatic classifier, EC, Model 3080L, and condensation particle counter, CPC, Model 3,075, TSI Inc., USA). The SMPS was operated with a sample flow of 0.5 l min⁻¹ and a sheath flow of 5 l min⁻¹ and measured mobility diameters (d_{mo}) from 11–470 nm. The scan times were set to 120 s with an additional 30 s of purge time added before each new scan cycle. All PSDs were corrected for dilution factors as well as diffusional losses within the sampling lines following methodology outlined in Hinds (1999).

2.4. Effective Density Measurements and Calculations

Combined measurements of particles' aerodynamic diameters (d_{ae}) and their corresponding d_{mo} enable determination of the corresponding particle masses (m) as described by Tavakoli and Olfert (2014),

$$m = \frac{\pi\rho_0}{6} \frac{C_c(d_{ae})d_{ae}^2 d_{mo}}{C_c(d_{mo})}, \quad (1)$$

where ρ_0 is 1,000 kg m⁻³ and C_c is the Cunningham slip correction factor. To perform particle mass measurements, an Aerodynamic Aerosol Classifier (AAC, Cambustion Ltd., UK), which could be bypassed, was installed upstream of the SMPS measuring PSDs. The AAC was used to size-select particles from the poly-disperse sample aerosol by aerodynamic diameter in the range between 50 and 250 nm. Continuous downstream SMPS measurements resulted in size distributions which were used to derive the corresponding d_{mo} . This was achieved by Gaussian least-squares fitting of the output data. In instances where multiple particle modes were observed in the SMPS data, which can suggest the presence of particles with different morphologies and compositions, multimodal Gaussian fits were applied (Figure S1 in Supporting Information S1). These modes were categorized into different particle types which are associated with particle modes in measured size distributions.

The effective density (ρ_{eff}) of a particle is defined as its mass divided by the volume of a sphere with a diameter equal to the particle's mobility diameter. Using this definition and combining it with Equation 1, it follows that,

$$\rho_{eff} = \frac{6m}{\pi d_{mo}^3} = \rho_0 \frac{C_c(d_{ae})d_{ae}^2}{C_c(d_{mo})d_{mo}^2}. \quad (2)$$

Due to instrumental limitations associated with both the SMPS and AAC, effective density measurements were limited to particles with $d_{ae} \geq 50$ nm.

2.5. Energy Dispersive X-Ray Fluorescence (EDXRF)

Trace element concentrations from PM_{2.5} (particulate matter ≤ 2.5 μm) collected on filters were measured using energy dispersive X-ray fluorescence (EDXRF) spectrometry. Samples were collected on 25 mm diameter Nuclepore™ track-etched membranes with a pore size of 0.4 μm (Whatman®) using a cyclone impactor with a 50% efficiency cut-off diameter of 2.5 μm . Sampling times varied between 25 and 75 min. EDXRF measurements were performed using a SPECTRO XEPOS analyzer (SPECTRO Analytical Instruments GmbH, Germany) controlled by the XRF Analyzer Pro software (AMETEK, USA). Each filter was analyzed at least three times. Moreover, all results were corrected for background values by analyzing blank filter membranes. Raw data output

was converted into element-specific emission factors by taking into account the sampling times, dilution factors and the fuel consumption for each individual filter.

2.6. Scanning Transmission X-Ray Microscopy (STXM) and Near-Edge X-Ray Absorption Fine Structure (NEXAFS)

More filter samples were collected for chemical mapping and X-ray microscopy imaging using a Sioutas five-stage cascade impactor and standard transmission electron microscopy (TEM) copper mesh grids (Ted Pella Inc.). All samples were collected on stages C and D at a flow rate of 9 l min^{-1} , resulting in a particle size range of $0.25\text{--}0.5\text{ }\mu\text{m}$ and $<0.25\text{ }\mu\text{m}$ respectively. These sampling times varied between 5 and 15 min.

Scanning transmission X-ray microscopy (STXM) coupled with near-edge X-ray absorption fine structure spectroscopy (NEXAFS) enables chemical analysis and morphological inspection of individual aerosol particles. The combined method results in detailed information of, for example, functional groups, particle mixing state and structure and morphology of sampled particles. In STXM-NEXAFS, the TEM grid samples are exposed to soft X-rays of adjustable energy inside a vacuum chamber. At energies close to the ionization threshold inner-shell electrons can absorb enough photons to be excited into unoccupied orbitals, which is referred to as absorption edge and is element specific (Moffet et al., 2010). These element- and energy-specific absorption edges help to identify the chemical composition(s) of samples, including the detection of specific functional groups. STXM measurements are conducted under high vacuum conditions, meaning there does exist the potential for volatile species to escape.

The STXM analysis was performed at the BL4U beamline at the UVSOR Synchrotron Facility in Okazaki, Japan and at the SoftiMAX beamline at MAX IV laboratory in Lund, Sweden. Both STXM beamlines cover energy ranges between 75 eV and 1 keV and 275 eV and 2.5 keV respectively, allowing measurements at the K-edges of carbon (280–300 eV), nitrogen (393–425 eV), oxygen (525–550 eV) and sodium (1,068–1,095 eV) as well as at the sulfur L-edge (159–196 eV).

Initial processing of data, such as image alignment, correction for background signal and conversion of flux data to optical density, was done using AXIS 2000 (Hitchcock Group Homepage, 2023).

2.7. Cloud Condensation Nuclei Counter (CCNC) Measurements and Calculations

The CCN activity of size-selected exhaust particles was determined using a single column CCN counter (CCNC; CCN-100, DMT). The supersaturation (SS) inside the growth chamber of the CCNC can be varied by either adjusting the sample flow rate (Q) or the stream-wise temperature gradient (ΔT). Details of the working principal are described in Roberts and Nenes (2005) and Lance et al. (2006). Exhaust particles were size-selected using a DMA (Model 3080L, TSI Inc., USA) covering a d_{mo} range between 50 and 250 nm. A CPC (Model 3,775, TSI Inc., USA) measured the total particle number concentrations (N_{p}) parallel to the CCNC to infer activated fractions (AF), that is the ratio between the number of activated particles and the total amount of particles.

During the engine experiments the CCNC was operated in Scanning Flow CCN Analysis (SFCA) mode (Moore & Nenes, 2009). This method allows for continuous measurements of SS spectra by ramping the sample flow rate while keeping ΔT constant. The sample flow rate was increased from 0.2 to 1.0 l min^{-1} at a constant rate for 120 s. At 0.2 and 1.0 l min^{-1} the sample flow was kept constant for 30 s. A mass flow controller (MFC) operated in parallel to the CCNC to maintain a total size-selected sample flow rate ($Q_{\text{CCNC}} + Q_{\text{MFC}}$) of 1.0 l min^{-1} . Supersaturation spectra were measured at $\Delta T = 4, 10$ and 18°C , resulting in a SS range of about $0.07\%\text{--}2.4\%$. Individual CCN spectra were visually inspected and multiple charging artifacts were accounted for by identification of pre-activation plateaus. Critical supersaturations (SS_c ; activation of 50% of the size-selected singly charged particle population into cloud droplets) were determined by fitting the measured activation curves to sigmoidal functions following Moore and Nenes (2009),

$$\frac{N_{\text{CCN}}}{N_{\text{p}}} = a_0 + \frac{a_1 - a_0}{1 + (Q_{\text{CCNC}}/Q_{50})^{-a_2}}, \quad (3)$$

where a_0 , a_1 , a_2 and Q_{50} are the minimum, maximum, slope, and inflection point respectively. Data were converted from Q_{50} to SS_c using linear fits derived from instrument calibrations (see Figure S2 in Supporting

Information S1). The CCNC was calibrated during the campaign using $(\text{NH}_4)_2\text{SO}_4$ particles generated from an aerosol generator (3079A, TSI Inc., USA).

The resulting SS_c values were converted to the dimensionless hygroscopicity parameter (κ) using,

$$\kappa = \frac{4A^3}{27d_{mo}^3 \ln^2(1 + SS_c/100\%)}, \text{ with } A = \frac{4\sigma_w M_w}{RT\rho_w}, \quad (4)$$

where SS_c is given in %, $\sigma_w = 71.99 \text{ mN m}^{-1}$ is the surface tension of water at 25°C , M_w is the molar mass of water, R is the universal gas constant, T is the absolute temperature and ρ_w is the density of water at 25°C ($\rho_w = 0.997 \text{ g cm}^{-3}$; Petters and Kreidenweis (2007)).

2.8. Ice Nucleation Measurements With the Portable Ice Nucleation Chamber II (PINCii)

The Portable Ice Nucleation Chamber II (PINCii) is a newly developed continuous flow diffusion chamber (CFDC) built to investigate ice nucleation by aerosol particles (Castarède et al., 2023). During measurements with PINCii, RH ramps for three to four pre-selected lamina temperatures were performed, that is, during each ramping cycle both wall temperatures are continuously adjusted so that the temperature in the sample flow lamina remains constant but the relative humidity with respect to ice (RH_i) is steadily increased. This method allows the temperature- and humidity-dependent ice nucleation onsets to be determined for aerosol particles over a wide range of conditions. Ramping experiments were performed at -26°C , -34°C (WS only), -38°C , -42°C (WS only) and -50°C and covered a RH_i range of 110%–160%. Size-resolved ice crystal concentrations were obtained from an optical particle counter (OPC; Remote 3,104, Lighthouse Worldwide Solutions, USA) at the PINCii outlet. The OPC has four size channels: (a) $0.3 \leq d_p < 1 \mu\text{m}$; (b) $1 \leq d_p < 3 \mu\text{m}$; (c) $3 \leq d_p < 5 \mu\text{m}$ and (d) $d_p > 5 \mu\text{m}$. Particle counts for size channels 3 and 4, that is, $d_p > 3 \mu\text{m}$, were considered as ice crystals in our results (Castarède et al., 2023). Between transitions to new lamina temperature settings, a solenoid valve at the inlet of PINCii switched to sample HEPA filtered ambient air for 15 min to measure background ice crystal concentrations and to correct values obtained from ramping experiments. Before entering PINCii, particles in the sample flow were dried using a diffusion dryer and size-selected using a DMA (Model 3080L, TSI, USA) to generate a monodisperse aerosol of $d_{mo} = 200 \text{ nm}$. Downstream of the DMA, the monodisperse sample flow was split and directed both toward PINCii and a CPC (Model 3,010, TSI, USA), which was used to infer activated fractions, that is, the ratio between measured ice crystals and the total particle concentration. Ice nucleation measurements were only performed during experiments with 50% engine load.

2.9. Calculation of Emission Factors

The amount of PN and PM emitted per kg of fuel burned were calculated as

$$EF_x = \frac{Q_{\text{exh}} C_x}{FC}, \quad (5)$$

where Q_{exh} is the exhaust gas flow in $\text{m}^3 \text{ h}^{-1}$, C_x is the number or mass concentration of a variable per m^3 , and FC is the load and fuel dependent fuel consumption in kg h^{-1} . To calculate particle number emission factors (EF_{PN}), particle size distributions were integrated and corrected for dilution factors and diffusional losses. Particle mass emission factors (EF_{PM}) were derived by either assuming a particle density of 1 g per cm^3 (EF_{PM,ρ_0}) or by using mean effective density values for individual size distribution modes ($EF_{\text{PM},\rho_{\text{eff}}}$), to give more realistic estimates. We want to stress that EF_{PM} estimates are only valid for mobility diameters smaller than 500 nm and thus, lead to a potentially non-negligible underestimate as particles of larger sizes, which are few in numbers but tend to dominate particle mass distributions, are generally co-emitted from these types of combustion engines (Fridell et al., 2008; Moldanová et al., 2009; Popovicheva et al., 2009).

In order to estimate CCN emission factors normalized by particle number concentrations and fuel consumption, a simple model approach as described by Kristensen et al. (2021) and Santos et al. (2023) is used. In this method, κ values for the entire size range of measured particle size distributions were derived by interpolating results obtained from CCNC measurements at distinct particle sizes. For particles smaller than 50 nm and larger than 150 nm κ values were kept constant at the respective threshold values. Interpolated κ values were subsequently

converted into critical supersaturations following Petters and Kreidenweis (2007), which allows activated fractions of CCN for individual size distributions at a given supersaturation to be calculated. Individual activated fractions are thereafter converted into CCN emission factors (EF_{CCN}) using,

$$EF_{CCN} = \frac{Q_{exh} N_{CCN}(SS)}{FC}, \quad (6)$$

where $N_{CCN}(SS)$ is the number concentration of CCN as a function of SS in $\# m^{-3}$, Q_{exh} is the exhaust gas flow in $m^3 h^{-1}$ and FC is the load and fuel dependent fuel consumption in $kg h^{-1}$.

3. Results and Discussion

3.1. Evaluation of Wet Scrubber SO_2 Removal Efficiency

Guidelines for exhaust gas cleaning systems outlined by the IMO mandate that ships utilizing exhaust wet scrubbers need to meet certain SO_2/CO_2 emission standards. If ships operate wet scrubbers outside of SECAs with fuels exceeding FSCs of 0.5%, the ratio between emitted SO_2 (in ppm) and CO_2 (in %) may not exceed a value of 21.7. In SECAs, where the maximum allowed FSC is limited to 0.1%, this ratio needs to be below 4.3 (IMO, 2021a).

During experiments performed at the 25% engine load point, the scrubber was able to reduce SO_2 to a ratio of at least 0.9 and consistently achieved SECA compliance levels. At 50% load, the ratio varied between 4.3 and 6.3, that is, a reduction to a SECA compliance level was possibly not reached. Similarly, at the highest load point of 75%, the SO_2/CO_2 ratio was reduced to 8.2, meaning that for the SO_2 measurement periods post scrubber, only global compliance could be achieved.

Determination of the scrubber's SO_2 removal efficiency was limited by sampling issues associated with the SO_2 monitor when measuring downstream of the scrubber. The high humidity in the sample air caused the gas monitor's condenser to deteriorate, which caused the measuring cell's pump to shut down. As a result, sampling downstream was limited to brief time periods, meaning that the SO_2 signal was often not stabilized before pump failure. Therefore, measured reduction values represent the minimum SO_2 reduction.

The SO_2 reduction efficiencies presented here exemplify limitations associated with the scaled down dimensions of the model wet scrubber used in this study. SECA compliance could not be achieved for all engine load points. However, a large fraction of ship traffic occurs on the open sea where ships do not have to adhere to SECA-related regulations. Wet scrubber related results we report in this study are therefore still valid for ocean-going vessels. Moreover, as stated in § 1, studies investigating the impacts of wet scrubbing on ship exhaust particle emissions show a wide range of effects. For real ships operating on the open sea, these combined factors mean there will be a wide envelope of operational conditions, employed emission systems and associated uncertainties.

3.2. Particle Size Distributions

Particle number size distributions measured with the SMPS for different engine load conditions are shown in Figure 2. Data displayed in the figure are averages of measurement periods where corresponding shaded areas depict measured uncertainties as \pm one standard deviation. In order to derive statistical information from the data, weighted non-linear least squares fits were applied (see Figures S6, S7 and S8 in Supporting Information S1). In some cases, fitting three modes to the size distributions reduced the residuals. Nevertheless, the discussion here is limited to uni- and/or bimodal modal fits.

The non-compliant HiS case shows at least one dominant mode between 18 and 25 nm and a second mode between 50 and 62 nm. Comparable size distributions have been measured, for example, by Kasper et al. (2007); Corbin et al. (2018) and Alanen et al. (2020) using a range of different engine and fuel types. In these cases, particles in the smaller mode probably originate from nucleation of volatile substances that are organic, inorganic or sulfurous in nature (Sippula et al., 2014). Particles in the larger mode often consist of mostly solid, fractal-like soot particles (Alanen et al., 2020; Anderson et al., 2015; Corbin et al., 2018).

When switching to the compliant LoS fuel, the measured size distributions changed significantly compared to HiS. The LoS size distributions are dominated by a single mode between 41 and 53 nm. Particles within this mode

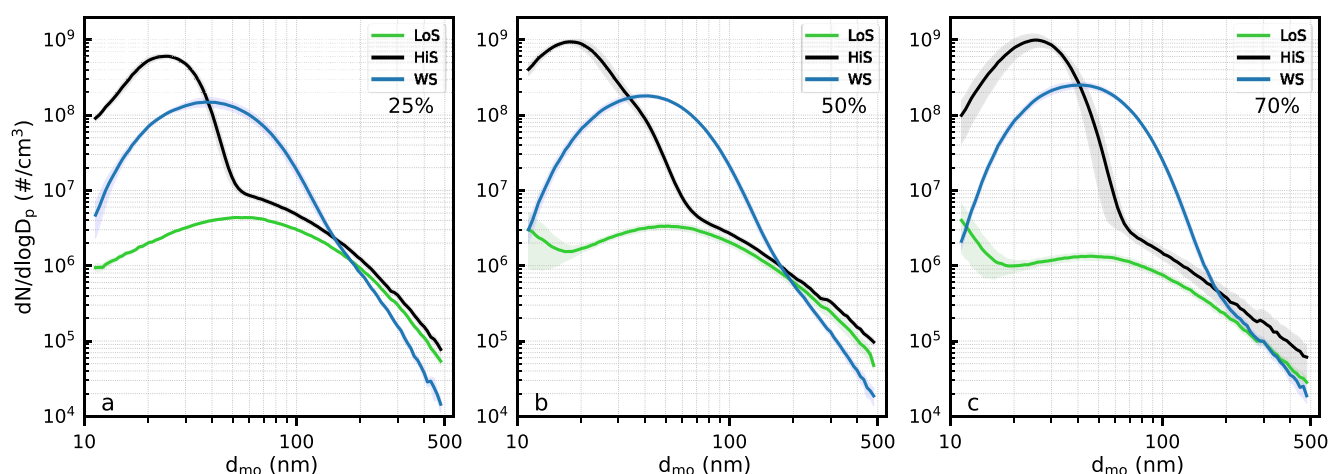


Figure 2. Average particle size distributions measured with the SMPS for the low FSC fuel (LoS), the high FSC fuel (HiS) and where HiS exhaust gas is passed through the wet scrubber using seawater (WS) are shown in panels (a) to (c). Respective panels show size distributions measured for 25%, 50% and 70% engine load regimes. The shaded areas depict \pm one standard deviation in measurement uncertainty. The fuel/case-specific size distributions are replotted in Figures S3 to S5 in Supporting Information S1 to facilitate engine load comparisons.

are most likely soot-type particles. The data also indicate the formation of nucleation mode particles below 20 nm and a related engine load dependence but are subject to large variability, which makes it difficult to draw conclusions. Moreover, the lower size limit of the SMPS model used in this study was ≈ 11 nm. Similar size distributions for low FSC fuels from marine test-bed engines have been reported by Anderson et al. (2015) and Santos et al. (2022).

While wet scrubbing maintained the bimodal characteristic of the HiS case, it also led to a shift in size of the dominant nucleation mode toward larger sizes and a reduction in the soot mode. A previous study conducted with the same wet scrubber but using a different engine, showed the formation of a particle mode around 20 nm. There the authors concluded that this was due to nucleation of sulfur-containing particles (Santos et al., 2022). However, size distributions for the non-compliant high FSC case, looked substantially different and lacked the dominant nucleation mode observed in this study. Similar observations regarding the shift in particle mode between pre- and post-scrubber, were also made by Jeong et al. (2023), who used a commercially available wet scrubber. Jeong et al. (2023) came to the conclusion that this shift in the size distribution was due to coagulation of primary and sulfur-containing particles in the scrubber.

Changes in engine load affect the particle size distributions in different ways. Soot modes are generally reduced in amplitude with increasing engine load as is the count median diameter of the respective modes with increasing engine load (Figures S3 to S5 in Supporting Information S1). While also being largely affected by general variations in combustion conditions, the amplitudes of nucleation mode particles (LoS), and the dominant particle mode in the HiS case, showcase an engine load dependence, where both amplitudes and count median diameter are strongly affected. In the LoS case, the amplitude increases with increasing engine load. The CMD and amplitudes of dominant particle modes in HiS, on the other hand, display much stronger variability with engine load (Figure S4 in Supporting Information S1).

3.3. Effective Densities

In Figures 3a–3c effective densities, ρ_{eff} , obtained from combined AAC and SMPS measurements, are shown for all cases and identified particle modes. More information about raw data output and processing, including determination of individual particle modes, can be found in Figure S1 and Figures S9 to S11 in Supporting Information S1.

Effective density values for LoS show a steady decline in ρ_{eff} with increasing mobility diameter (Figure 3). This behavior is typical for soot particles, as the structure and morphology of exhaust particles become less dense with increasing size, as has been reported in diesel engine studies (Momenimovahed et al., 2021; Olfert et al., 2007; Olfert & Rogak, 2019; Park et al., 2003; Rissler et al., 2013; Trivanovic et al., 2019). From the ρ_{eff} trends, one can

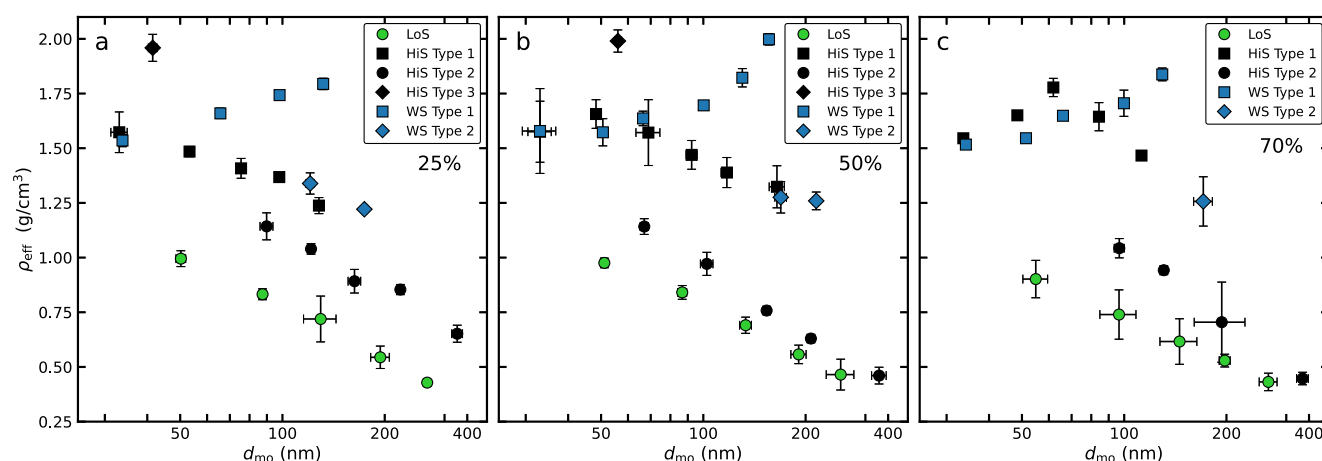


Figure 3. Measured effective densities (ρ_{eff}) for the fuels LoS and HiS and the HiS + wet scrubber case as a function of particle mobility diameter for engine load regimes of (a) 25%, (b) 50% and (c) 70%. Error bars represent \pm two standard deviations. Classification into different particle types was based on observed trends in the raw data output (see Figures S9 to S11 in Supporting Information S1). Particle types generally coincide with particle modes in measured size distributions (see Figure 2 and Figures S6 to S8 in Supporting Information S1).

derive the mass-mobility relationship according to Park et al. (2003), where the fractal dimension, D_f , is indicative of the morphology of the exhaust particles. A homogeneous, spherical particle, for example, has $D_f = 3$, whereas diesel engine exhaust particles typically yield values between 2.2 and 2.8 (Olfert et al., 2007; Olfert & Rogak, 2019; Park et al., 2003; Rissler et al., 2013; Trivanovic et al., 2019). Analysis of the mass-mobility relationship for LoS particles revealed no clear dependence of D_f on the engine load as the value remains at 2.56 (Figure S12 in Supporting Information S1).

Particles from HiS combustion display different trends in ρ_{eff} compared to LoS. First, at least three different particle types were classified. The different types remained after SMPS data were corrected for multiple charging artifacts and also coincide with the different particle modes observed in the measured particle size distributions (HiS; Figure 2 and Figure S7 in Supporting Information S1). Effective densities of HiS particles of the first type (up to 165 nm) generally ranged between 1.24 and 1.78 g cm^{-3} between all load points and sizes and showed no clear trends between 30 and 100 nm, making it difficult to assess whether those are spherical or fractal-like aggregates. Results also indicate a general increase with engine load. An immediate comparison between LoS and HiS can be drawn when looking at density values for HiS's second type which shows a significant increase in ρ_{eff} compared to LoS. Density values of the second type show a clear decreasing trend with increasing size which indicates a soot mode and range between 1.14 and 0.65 g cm^{-3} (25% load), 1.14 and 0.46 g cm^{-3} (50% load), and 1.04 and 0.45 g cm^{-3} (70% load; Note that in this case, the smallest measurable size was 97 nm). Mass-mobility analysis of HiS Type 2 particles indicates that particles become less dense with increasing engine load as D_f decreases from 2.60 (25% load) to 2.35 (70% load; see Figure S13 in Supporting Information S1). Measurements by Olfert et al. (2007) showed that in the presence of high sulfate concentrations, effective densities could increase dramatically due to potential condensation of sulfuric acid which has a material density of 1.84 g cm^{-3} . As for the third observed type, ρ_{eff} varied between $1.96 \pm 0.06 \text{ g cm}^{-3}$ (25%) and $1.99 \pm 0.05 \text{ g cm}^{-3}$ (50%) which is larger than the density of sulfuric acid but within the range of the proposed mean value for particles produced from liquid fuels with low organic content, $1.834 \pm 0.187 \text{ g cm}^{-3}$ (Ouf et al., 2019).

Changes in particle number size distributions due to wet scrubbing are also reflected in ρ_{eff} . Two distinct WS particle behaviors were identified from the analysis and are present at all three load points. For particles between ≈ 34 and ≈ 130 nm ρ_{eff} increased from 1.56 to 1.82 g cm^{-3} (averaged over all load points). At the low end of this range ≤ 90 nm the ρ_{eff} WS and HiS values predominantly overlap at the higher load points. At 25% load HiS and WS results diverge except for the smallest particles (34 nm). Furthermore, effective density values captured for WS exhaust suggest that the particle types could potentially be very similar to those emitted from HiS combustion in terms of composition and morphology. It should be stated, that the type assignment during the analysis steps does not necessarily exclude any misclassification or overlap between types and size modes, as indicated by the agreement of WS second type particles and the largest measured effective densities for Type 1 HiS particles.

Table 2
Summary of Particulate Matter Related Emission Factors Measured for the Three Different Cases and Engine Loads Normalized by Load-Dependent Fuel Consumption

Case	Load	S $\mu\text{g kg}^{-1}$	Cl $\mu\text{g kg}^{-1}$	K $\mu\text{g kg}^{-1}$	Ca $\mu\text{g kg}^{-1}$	Fe $\mu\text{g kg}^{-1}$
LoS	25	0.92 ± 0.32	0.10 ± 0.07	0.03 ± 0.02	0.19 ± 0.10	0.33 ± 0.18
	50	0.36 ± 0.13	0.00 ± 0.01	0.00 ± 0.00	0.04 ± 0.02	0.13 ± 0.07
	70	0.18 ± 0.07	0.02 ± 0.01	0.01 ± 0.01	0.02 ± 0.01	0.06 ± 0.04
HiS	25	23.13 ± 5.98	0.03 ± 0.01	0.02 ± 0.01	0.15 ± 0.09	0.33 ± 0.23
	50	20.71 ± 5.89	0.00 ± 0.00	0.05 ± 0.02	0.30 ± 0.10	0.50 ± 0.20
	70	24.91 ± 6.29	0.01 ± 0.01	0.00 ± 0.00	0.09 ± 0.04	0.40 ± 0.14
WS	25	38.63 ± 9.45	1.25 ± 0.32	0.14 ± 0.09	0.51 ± 0.17	0.51 ± 0.25
	50	38.23 ± 9.70	0.95 ± 0.28	0.32 ± 0.10	0.66 ± 0.19	0.62 ± 0.18
	70	31.14 ± 8.39	0.60 ± 0.16	0.07 ± 0.04	0.31 ± 0.09	0.93 ± 0.29

Note. Emission factors of S, Cl, K, Ca and Fe were derived from filter-based EDXRF measurements of PM_{2.5} sampled using a cyclone impactor. The uncertainties are given as \pm two standard deviations.

3.4. Chemical Characterization-EDXRF and STXM Analysis

Table 2 summarizes emission factors normalized by fuel consumption for selected elements derived from EDXRF analysis of PM_{2.5} filters. Emissions of sulfur are significantly reduced at lower FSCs. Since the fuel compositions of HiS and LoS mainly vary in terms of sulfur content and engine parameters for various engine load points were replicated for all cases, we can conclude that the difference in sulfur emissions is mainly driven by enhanced emissions of sulfur containing particles when using HiS fuel, either due to nucleation of new particles containing sulfur species or due to coating of soot particles. The sulfur in the LoS case may originate from the relatively small amount of FSC or a potential non-negligible sulfur content in the lubrication oil. The lubricant oil used during experiments, Volvo VDS-4.5, may contain up to 0.4% sulfur by mass. Sulfur emission factors in the particulate phase are increased when HiS exhaust is passed through the wet scrubber. While no load dependence is apparent, particle sulfur emissions are increased on average by 59% when the scrubber is used. This result supports the hypotheses, that the scrubbing can lead to coagulation of nucleated sulfur-containing particles or lead to enhanced surface uptake of sulfur species by primary exhaust particles. These results agree with observations made by Yang et al. (2021), who found wet scrubbing to be inefficient in removing sulfate particles, and Jeong et al. (2023), who observed coagulation of sulfate particles downstream of a wet scrubber. We cannot exclude the presence of other sulfur-containing particles not captured by the SMPS measurements.

Wet scrubbing was also found to enhance emissions of chlorine, potassium, calcium and iron. While the chlorine, potassium and calcium are linked to the composition of the seawater used for the scrubbing process, enhanced iron concentrations may have originated from corrosion of scrubber and or exhaust-pipe components. We cannot exclude the potential for scrubbing processes to lead to enhanced external mixing of particulate or to influence microphysical processes affecting chemical compositions.

Other elements that are often used as tracers for different fuel types, such as vanadium for high FSC residual fuel oils (Moldanová et al., 2009, 2013; Popovicheva et al., 2009), were either found to be around background levels or below detection limits in all cases.

Complimentary STXM and NEXAFS analyses show that different cases resulted in different mixing states characterized by a few distinct particle types. For LoS sample grids mainly carbonaceous, soot like particles were observed, although we cannot fully exclude that other combustion-related particles are present. Figure 4 shows (a) a typical soot particle and corresponding NEXAFS spectra at (b) the carbon K-edge and (c) the oxygen K-edge. The peak observed at ≈ 285.4 eV is characteristic for doubly bonded carbon and is also referred to as a “graphitic peak” and has been documented for soot particles from different combustion sources (Braun, 2005; di Stasio & Braun, 2006; Moffet et al., 2010; Alpert et al., 2017; Mahrt, Alpert, et al., 2020). A broad absorption feature starting at around 291 eV is characteristic of the C–C single bond. The oxygen K-edge shown in panel c indicates the presence of the carbonyl group in the particle as indicated by the sharp and broad peaks at ≈ 531 and ≈ 538 eV

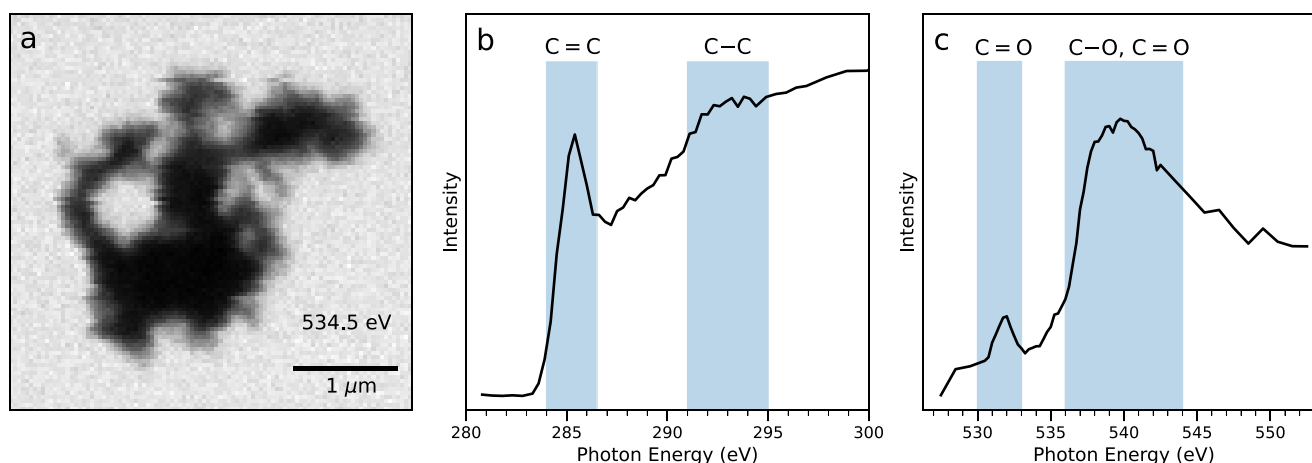


Figure 4. A scanning transmission X-ray microscopy (STXM) image and corresponding near-edge absorption fine structure (NEXAFS) spectra of a typical LoS exhaust particle. (a) A X-ray microscopy image taken of the respective particle at the oxygen K-Edge at 534.5 eV. NEXAFS spectra acquired for the particle at (b) the carbon K-edge and (c) the oxygen K-edge. The blue shaded areas in panel (b) and (c) mark absorption features related to the different functional groups displayed over the corresponding areas. The ranges for the shaded areas were visually estimated from Moffet et al. (2010).

respectively (Moffet et al., 2010; Tivanski et al., 2007). Oxygenated functional groups, such as the carbonyl group, originate from reactions with oxygen during the combustion process.

For HiS exhaust, two distinct particle compositions were observed which were identified as soot and sulfate (Figure 5a). In Figure 5b the soot NEXAFS spectrum has a peak at around 532 eV corresponding to the carbonyl group, which is missing for the sulfate. Both spectra show a distinct peak above 537 eV, which signals the presence of sulfate particles and soot containing sulfate (Fauré et al., 2023; Kong, Gladich, et al., 2023; Zelenay et al., 2011). This peak is broader for the soot particle, which indicates the presence of oxygen atoms bonded to carbon atoms but other compounds cannot be excluded due to the complexity of this absorption region. The nitrogen K-edge spectrum for the sulfate particle shows two distinct absorption features which have been previously observed for ammonium sulfate particles by Leinweber et al. (2007), although a presence of nitrate in the nitrogen K-edge spectrum of the sulfate particle cannot be excluded (Kong, Priestley, et al., 2023; Weeraratna et al., 2022). No nitrogen was associated with the soot particle. The sulfur L-edge spectrum of the sulfate particle (Figure 5c) shows characteristic peaks between 170 and 185 eV which align with those measured for sodium sulfate particles by Sarret et al. (1999). Experimental constraints did not allow for a sulfur spectrum to be acquired for HiS soot particles but a direct comparison of oxygen K-Edge spectra between the LoS and HiS soot particles (Figures S14 in Supporting Information S1) shows distinct spectral differences between 536 and 539 eV. The oxygen spectrum of the HiS soot particle shows a sharp increase in absorption at ≈ 536 eV which coincides with the spectrum of the HiS sulfate particle. For the LoS soot particle, a similar absorption feature is shifted toward higher energies of ≈ 538 eV. Similar variations in oxygen NEXAFS spectra for fresh soot and sulfuric acid aged soot have been observed. There, the authors conclude that the shift in signal toward lower energies for the aged soot originates from sulfate on the soot particle (Priestley et al., 2023).

In Figure 6a an overview snapshot of WS particles at a single energy of 285.8 eV (carbon absorption edge), displays different particle types, which were consistent for all WS samples. A differential image, which was produced by aligning two images of different energies (pre- and post-sodium K-edge) and subtracting the signal of the pre-edge image from the post-edge signal (Figure 6b; 1,071–1,065 eV) highlights the presence of cubic-shaped sodium chloride particles. A similar image at the oxygen K-edge (537.5–530.5 eV; Figure 6c) shows fractal-like, oxygen containing particles highlighted in blue and column-shaped mineral particles (calcium sulfate, CaSO_4), as well as other oxygen-containing particles in orange. In the WS samples, isolated soot or mineral particles were rarely observed and often surrounded salt particles. One explanation for this is that the aforementioned particles were immersed in saline solution droplets during the sampling process. The water subsequently evaporated during storage or STXM analysis, leaving behind crystallized salt particles with attached soot and mineral particles. Similar heterogeneous particle mixtures have been observed in exhaust utilizing the same

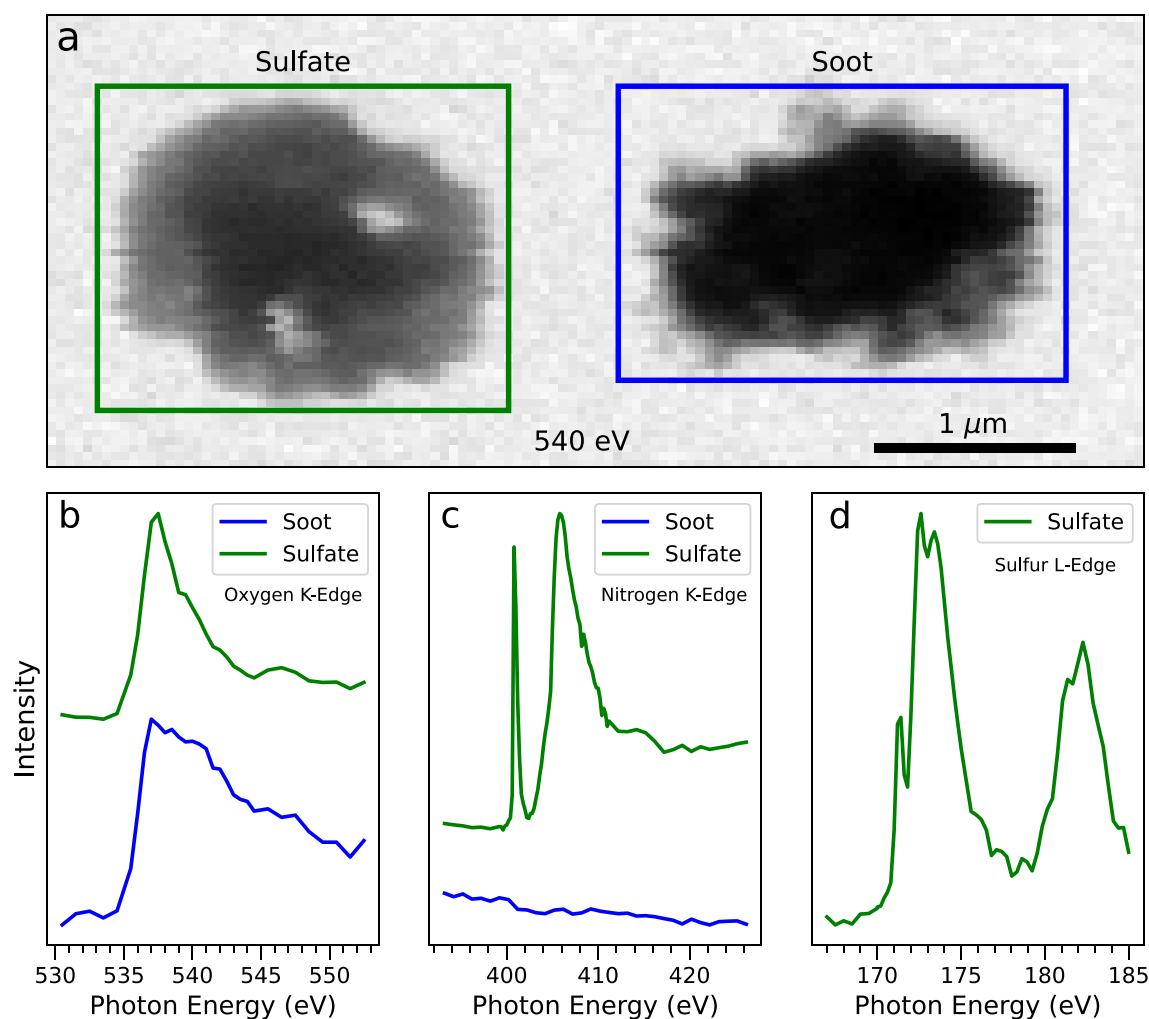


Figure 5. STXM image and NEXAFS spectra from HiS exhaust particles. (a) STXM images taken at 540 eV showing sulfate-type and soot particles. NEXAFS spectra at (b) the oxygen K-edge, (c) the nitrogen K-edge and (d) the Sulfur L-edge. Spectra shown in panels (b) to (d) represent the average of whole particles, although during the analysis process all particles were inspected for spectral heterogeneity.

scrubber but with a different engine (Santos et al., 2023). Similar to HiS emissions, sulfate particles were also encountered for the WS case (see Figure S15 in Supporting Information S1).

3.5. CCN Activity

The calculated hygroscopicity parameter, κ , for all cases, engine loads and particle sizes between 50 and 250 nm is displayed in Figure 7. Combustion of HiS fuel resulted in emissions of particles with relatively high hygroscopicities. The κ value of 50 nm particles varied between 0.661 and 0.649 with no apparent engine load trend. These values are comparable to those of sulfur-containing, inorganic species, such as ammonium sulfate, which has a κ -value of 0.61 (Petters & Kreidenweis, 2007) and to those of exhaust particles from ships utilizing fuels with a FSC >0.5%, which has been estimated to be around 0.63 (Yu et al., 2020, 2023). In general, the hygroscopicity of HiS exhaust particles decreases with increasing particle size. However, at 75 nm, κ values are substantially smaller than for 50 or 100 nm particles. This may be due to an overlap of different particle types of varying hygroscopicity, which could not be clearly resolved in the activation spectra. Beyond 100 nm a steady decrease in κ is observed with increasing particle size, which supports the hypothesis that particle emissions around 50 nm and larger than 100 nm are dominated by emissions of sulfate and soot respectively.

The hygroscopicity of exhaust particles is strongly affected by FSC reduction as can be seen from the significantly reduced κ values of LoS particles. At 50 nm, κ is reduced to 0.035–0.079. These hygroscopicities agree with

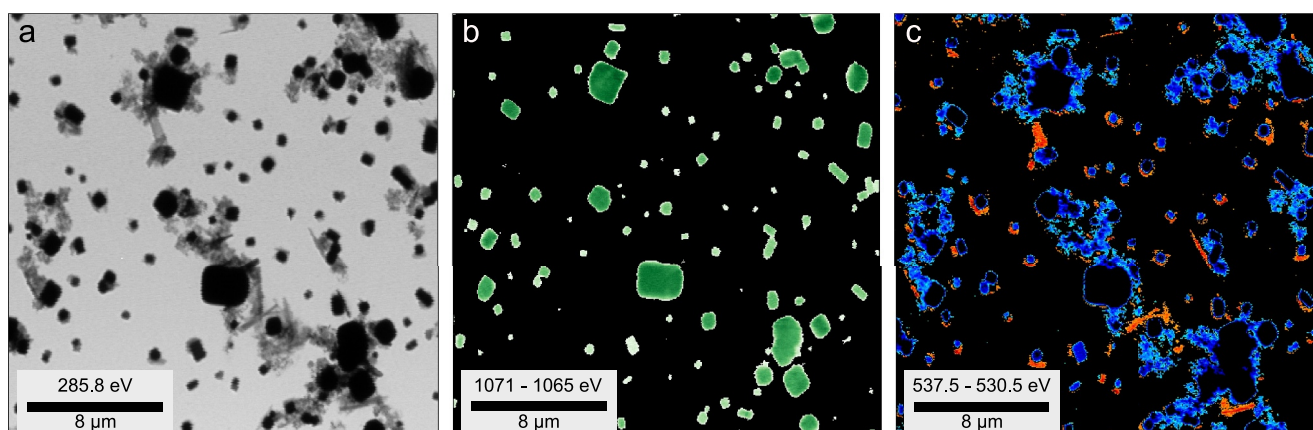


Figure 6. STXM images of particles from wet scrubber exhaust taken at different energies. (a) Single energy image around the carbon K-Edge (285.8 eV) showing different particle morphologies present on the grid. (b) Differential energy image at the sodium K-Edge (1,071–1,065 eV), where different shades of green indicate the intensity of the measured Na signal. (c) Differential energy image at the oxygen K-Edge (537.5–530.5 eV), where hues of red indicate the presence of oxygen-rich sulfates and mineral particles and bluish hues highlight oxygen-containing soot particles. In (b) and (c) images taken within the same absorption edge were pixel-aligned and background corrected. Signals of the lower (pre-edge) energies were subtracted from signals obtained at absorption peaks (higher energy values). The choice of the two respective energy values were based on carbon and sodium NEXAFS spectra typical for the respective particle types.

measurements from other diesel engine studies of unaged soot particles (Henning et al., 2012; Korhonen et al., 2022; Wittbom et al., 2014). The strong reduction in hygroscopicity compared to HiS was observed for all measured particle sizes as κ continues to decrease monotonically with increasing particle size. The large difference in κ between HiS and LoS can be explained by the absence of sulfate particles and sulfate on soot particles, which can increase hygroscopicity of generally hydrophobic soot particles. No clear correlation between hygroscopicity and engine load was found.

The effect of wet scrubbing on κ values is mostly seen in the size range 50–100 nm. These changes also coincide with the shifts in the dominant particle modes toward larger sizes which is shown in Figure 2 and the changes in ρ_{eff} for WS particles (Figure 3). For all three engine loads, the hygroscopicities of WS particles between 50 and 100 nm did not display any clear size-dependence. The average values for this size range vary between 0.65 and 0.74 with no clear engine load dependence. It was found that the κ values of 50 nm WS particles were very similar to those of 50 nm particles originating from HiS combustion. Taking into account the similarities in ρ_{eff} for the same size range and the results obtained from the chemical characterization, we can hypothesize that 50 nm

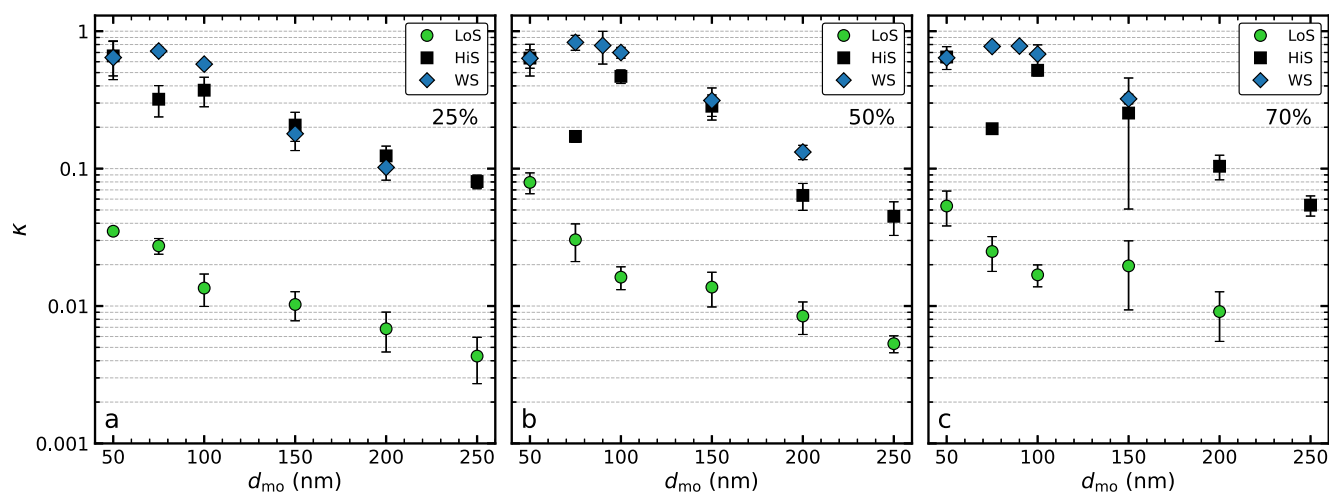


Figure 7. CCN activity expressed as the mean hygroscopicity parameter (κ) value for particle mobility diameters between 50 and 250 nm. LoS represents combustion of low FSC fuel, HiS of non-compliant high FSC fuel and in WS, HiS exhaust was processed by the wet scrubber. Panels (a) to (c) show results for engine loads ranging from 25% to 70% (as indicated). The error bars represent \pm two standard deviations of measurement uncertainty. All κ values were calculated from measured critical supersaturations (see Figure S16 in Supporting Information S1).

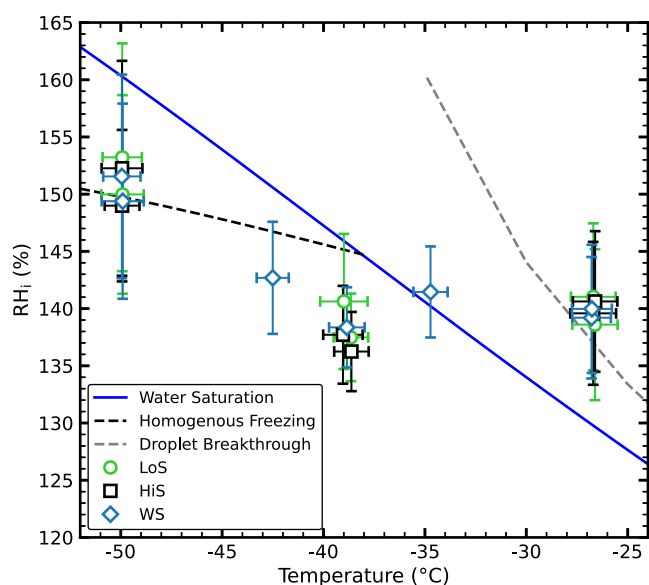


Figure 8. Summary of 200 nm particle freezing experiments over a range of -50 to -26°C . Freezing onsets were determined where the frozen fraction between ice crystals ($>3\ \mu\text{m}$) and the total particle number concentrations exceeded 1%. The solid blue line indicates water saturation, the dashed black line represents the homogeneous freezing threshold for 200 nm particles according to Koop et al. (2000) (calculated with a water activity (Δa_w) of 0.2946) and the gray dashed line represents the experimentally determined droplet breakthrough conditions of PINCii (Castarède et al., 2023).

particles in both cases are similar. Above 100 nm, κ values of WS particles decrease steadily to values of 0.102 (25%) and 0.132 (50%) at 200 nm. The different trends in κ below and above 100 nm suggest that wet scrubber particle emissions are characterized by more hygroscopic (<100 nm) and less hygroscopic particles (>100 nm). Values in the smaller size range indicate the presence of inorganic species (Petters & Kreidenweis, 2007), and given results shown in Figures 2 and 3, suggest the presence of sulfate particles. Larger particles show a steady decrease in κ with increasing particle size which has previously been reported by Santos et al. (2023) and could stem from soot particles with substantial amounts of sulfate.

3.6. IN Activity

Onset conditions for ice nucleation at a given temperature and relative humidity with respect to ice, RH_i , for 50% engine load experiments are presented in Figure 8. The onset conditions were determined when activated fractions exceeded 1%, determined by calculating the ratio between the sum of all OPC channels $\geq 3\ \mu\text{m}$ and the total particle numbers detected by the CPC measuring in parallel with PINCii. In contrast to the results obtained from CCN activity measurements, ice nucleation onsets do not vary with fuel type or exhaust wet scrubbing. At temperatures warmer than required for homogeneous freezing, ice nucleation was not observed below water saturation. Data collected at around -26°C show that all onsets are around droplet breakthrough conditions (gray dashed line), which was experimentally determined for various PINCii operating conditions by Castarède et al. (2023). Droplet breakthrough characterizes a threshold in the T - RH_i parameter space wherein unfrozen droplets continue to grow to detectable

sizes for the OPC, thus inhibiting phase discrimination. At temperatures between ≈ -34 and -43°C , freezing onset occurs below homogeneous freezing conditions, which has previously been reported for soot particles coated with different acids (Friedman et al., 2011) and agrees with measurements by (Möhler et al., 2005). In Santos et al. (2023), the authors found that the fuel aromatic content had a major influence on the exhaust particles' ability to form liquid droplets. It is therefore possible that aromatics may also facilitate freezing of fresh soot particles. Organics and sulfuric acid in the particle phase can have a large influence on the IN ability of soot particles, for example, by filling pores and thus, inhibiting pore condensation freezing, or by increasing particles' hygroscopicities due to sulfuric acid coatings (Gao & Kanji, 2022).

If wet scrubbing of exhaust particles is seen as a type of cloud conditioning, then it might enable heterogeneous freezing at warmer temperatures and/or lower supersaturations as has been demonstrated by Mahrt, Kilchhofer, et al. (2020). Nevertheless, uncertainties in RH_i are pronounced, making it difficult to determine precisely the RH of the freezing onsets. It is also worth noting that at $T = -50^{\circ}\text{C}$ ice crystal growth of 200 nm sample particles to sizes above $3\ \mu\text{m}$ is significantly limited by the residence time inside PINCii's growth chamber and requires RH_i above 150% (Figure S17 in Supporting Information S1). This can introduce an additional uncertainty when performing measurements at low temperatures. In Castarède et al. (2023), the authors show an alternative way to visualize freezing onsets of aerosol particles using PINCii. This approach takes into account the fact that homogeneous freezing is an irreversible process. Once ice formation is triggered, ice crystals continue to grow even if their remaining trajectory inside the growth chamber has less favorable freezing conditions. Here, we employ this alternative method to determine freezing onsets based on maximum RH_i values in the flow lamina. Results utilizing this alternative approach are presented in Figure S18 in Supporting Information S1 and suggest that most data reflect homogeneous or even more extreme freezing conditions.

3.7. Emission Factors-PN, PM and CCN

Emission factors normalized by fuel consumption for particles derived from SMPS measurements (11–470 nm) are shown in Table 3. In general, particle number emission factors (EF_{PN}) varied between 0.33×10^{14} and $80.68 \times 10^{14}\ \text{kg}^{-1}$. A strong reduction in EF_{PN} was observed when switching from non-compliant HiS to SECA-compliant LoS, which agrees with other studies that have shown large reductions in particle number emissions

Table 3
Summary of Particulate Matter Related Emission Factors Measured for the Three Fuel Cases and Engine Loads Normalized by Load-Dependent Fuel Consumption

Case	Load	EF_{PN} $10^{14} \# \text{ kg}^{-1}$	EF_{PM,ρ_0} (1) mg kg^{-1}	$EF_{PM,\rho_{\text{eff}}}$ (2) mg kg^{-1}	$EF_{CCN,0.3\%}$ $10^{13} \# \text{ kg}^{-1}$	$EF_{CCN,0.7\%}$ $10^{13} \# \text{ kg}^{-1}$
LoS	25	1.18 ± 0.04	84.70 ± 3.20	62.49 ± 2.36	0.20	1.13
	50	0.73 ± 0.23	48.76 ± 14.75	34.70 ± 10.50	0.18	0.75
	70	0.33 ± 0.33	16.88 ± 3.29	11.08 ± 2.16	0.08	0.29
HiS	25	69.90 ± 8.90	181.92 ± 28.94	198.23 ± 32.08	7.19	51.76
	50	80.68 ± 14.55	111.23 ± 21.91	126.01 ± 28.73	3.22	33.27
	70	77.52 ± 30.11	116.35 ± 30.50	164.58 ± 44.30	1.76	77.32
WS	25	26.93 ± 5.11	238.48 ± 63.26	388.36 ± 105.96	43.22	146.75
	50	23.44 ± 2.73	201.14 ± 18.62	333.14 ± 31.17	38.77	136.26
	70	28.19 ± 4.83	218.20 ± 18.25	358.92 ± 30.05	45.41	166.25

Note. Particle number (EF_{PN}) and particle mass emission factors (EF_{PM}) are derived from integration of measured particle size distributions between 11 and 470 nm. Moreover, EF_{PM} are calculated (1) assuming unit density for all particles (EF_{PM,ρ_0}) and (2) using the average ρ_{eff} for individual particle modes ($EF_{PM,\rho_{\text{eff}}}$). The uncertainties are given as \pm two standard deviations.

due to FSC reductions (Seppälä et al., 2021; Yu et al., 2020, 2023; Wu et al., 2020). On average EF_{PN} were reduced by 99%, which can be largely attributed to the absence of sulfate aerosol smaller than 50 nm. Nevertheless, soot mode particles were also reduced when using LoS fuel (see Figure 2). During WS experiments, emissions were on average reduced by 65% compared to HiS which is within the range of other studies investigating the effects of wet scrubbers on PN emissions from marine engines (Fridell & Salo, 2016; Lehtoranta et al., 2019; Winnes et al., 2020; Yang et al., 2021). Contrastingly in a previous study, that utilized the same scrubber but a different engine, wet scrubbing led to an increase in EF_{PN} (Santos et al., 2022). The change in emission behavior compared to Santos et al., (2022) may have different sources, including general differences in the emission profiles between engines or the addition of packing material between scrubber demister plates that was not utilized in the earlier study. Nevertheless, results presented in this study show that such simplified model scrubbers may be useful in investigating effects of wet scrubbing on exhaust PM emissions and can be used for further research and development of the technology. A clear load dependence was only observed for LoS where EF_{PN} are steadily reduced with increasing engine load.

Particle mass emission factors show diverging trends for the alternative compliance measures. For LoS fuel, EF_{PM} are reduced on average by 65% and 75% when either assuming unit density for all particles (EF_{PM,ρ_0}) or when using average ρ_{eff} values for individual particle modes ($EF_{PM,\rho_{\text{eff}}}$). Wet scrubbing led to a reduction in particle numbers but EF_{PM,ρ_0} and $EF_{PM,\rho_{\text{eff}}}$ increased by 67% and 126% compared to the respective HiS cases. As can be seen in Figure 2, scrubbing led to a decrease in the soot mode but this removal of large particles is compensated by the shift in the ultrafine, sulfate mode. Similar to EF_{PN} results, a clear engine load dependence was only observed for LoS where emissions decrease with increasing engine load.

The importance of including particle type differences and morphologies when estimating EF_{PM} from SMPS measurements is highlighted when the differences for individual cases are compared. For the soot particles that are emitted from LoS combustion, decreasing trends in ρ_{eff} are reflected in reduced EF_{PM,ρ_0} . On the other hand, sulfates, salts and generally more dense particles, have material densities larger than 1 g cm^{-3} and often do not possess fractal structures like soot particles, thus leading to relative increases in EF_{PM} for HiS and WS.

Estimated CCN emission factors (EF_{CCN}) for atmospherically relevant supersaturations of 0.3% and 0.7% are shown in Table 3. The full spectrum of EF_{CCN} for a supersaturation range of 0%–1% is shown in Figure S19 in Supporting Information S1. During the interpolation process to derive size-dependent critical supersaturation values of HiS particles, κ values at 75 nm were excluded due to the previously discussed uncertainties.

Estimates show different EF_{CCN} trends for the competing compliance pathways when compared to HiS. At both $SS = 0.3\%$ and 0.7% CCN emissions are substantially reduced for LoS across all load points. On average CCN

emissions are reduced by 97% due to the switch to the low FSC fuel for both *SS* values with little variation across engine loads. Similar CCN reductions from ships operating on low FSC fuels were observed by Yu et al. (2020, 2023). Wet scrubbing, on the other hand, was found to lead to a substantial increase in EF_{CCN} when compared to HiS. Compared to a previous study conducted with the same scrubber where no clear increase in CCN emissions was found (Santos et al., 2023), here, scrubbing induced shifts in the particle size distributions toward larger sizes, strongly impact EF_{CCN} . While κ values for HiS and WS are similar and particles larger than ≈ 200 nm are reduced from scrubbing, the increase in CCN emissions for the WS case is dominated by substantially increased particle concentrations in the range of 50–100 nm.

4. Summary and Implications

In this study, a diesel engine was used to investigate how present international marine fuel regulations impact physicochemical properties and the cloud activity of exhaust particles. We investigated two regulatory compliance measures aimed at sulfur emission reductions. Those are, direct fuel sulfur content reduction and exhaust wet scrubbing. Aerosol instrumentation was used to measure size distributions and effective densities of emitted exhaust particles as well as their liquid droplet and ice crystal forming abilities. Energy dispersive X-ray fluorescence and scanning transmission X-ray microscopy were used to characterize chemical compositions and exhaust particle mixing states. This study found that compliance measures have significant impacts on particulate emission profiles with relevant implications for atmospheric processes and human health. Our key findings are.

- Combustion of low sulfur content fuel resulted in significant reductions of ultrafine particulate emissions, most likely due to the absence of sulfate particles in the range of 20–30 nm. In this case, particulate emissions are dominated by soot particles.
- While soot mode particles were reduced, wet scrubbing was found to shift sulfate mode particles toward larger sizes, possibly due to coagulation. This shift in the sulfate mode is supported by results from EDXRF measurements, where we see significant increases in particulate sulfur emissions from wet scrubbing compared to the non-compliant fuel.
- Changes in the mixing state of the particles are also reflected in their hygroscopicities. Low sulfur fuel combustion primarily led to particle emissions of low hygroscopicity, resulting in strong CCN emission reductions compared to non-compliant high sulfur content fuel. Wet scrubbing, on the other hand, increased CCN emissions substantially, most likely caused by changes in the particle size distributions and/or due to possible transfer and condensation of water-soluble compounds onto exhaust soot particles.
- While we found compliance measures affect exhaust particles' hygroscopicities, no significant impact on ice nucleation was observed. Potential changes in the mixing state of 200 nm wet scrubber exhaust particles, did not improve ice nucleation abilities of particles. Fresh soot-type particles remain inefficient ice nucleating particles.
- With the exception of particle size distributions and consequently, particle number and mass emission factors, no obvious engine load dependencies were found for other parameters, such as the effective densities and the CCN activity of exhaust particles. We observed that soot mode particles are clearly reduced with increasing engine load. This was not the case for sulfates within the ultrafine mode.
- The scaled-down model wet scrubber affected the SO_2 removal efficiency, and therefore did not achieve SECA compliance at all engine loads. Nevertheless, we do not anticipate a further minor reduction in SO_2 emissions to affect particle emission properties substantially, as results obtained at an 25% engine load agree well with those obtained at higher load points. Moreover, a large fraction of shipping activity occurs in regions where ships are not required to comply with SECA regulations, therefore, our results remain valid for most shipping activity.

Despite efforts to reduce particulate emissions to the atmosphere, maritime transport remains a significant source. A variety of fuel types and exhaust aftertreatment systems are emerging, as marine regulations evolve. Studying these emissions remains an important research question. This study shows that two alternative solutions to comply with emission control regulations have significant impacts on properties of exhaust particles. These types of results have implications for human health, for example, by reducing or increasing the burden of submicron particle emissions close to populated areas, affected by ship traffic, but can also have climate-related consequences. While we only studied those effects on fresh exhaust particles, once emitted to the atmosphere, particles undergo chemical and physical processing that can influence their interaction potential within the atmosphere (Khalizov et al., 2009; Mahrt, Alpert, et al., 2020a; Wittbom et al., 2014). The Arctic is an interesting study area,

where unique feedback mechanisms lead to amplified warming rates and to steadily decreasing sea ice extent. Increasing shipping activity is a projected future result (Peters et al., 2011). In such pristine environments, where background aerosol concentrations are generally low, aerosol introduced by ships may cause strong local responses in the Earth-atmosphere system. Anticipating potential risks posed by growing shipping activity, ongoing initiatives are focused on reducing its environmental footprint. For example, from 2024 and onwards ships in the Arctic will no longer be allowed to use heavy fuel oils or, in general, fuels with densities and kinematic viscosities exceeding 900 kg m^{-3} and $150 \text{ mm}^2 \text{ s}^{-1}$ respectively (IMO, 2021b). Regulations like these will most likely reduce wet scrubber usage in the Arctic and also alter exhaust emissions of particulate matter from ships in Arctic waters. To this day, large uncertainties in quantifying aerosol-cloud interactions and especially, the effect of maritime shipping on radiative forcing, still prevail (IPCC, 2021). The results presented in this study, including information on exhaust particle size distributions, associated hygroscopicity values and emission factors, can be useful input parameters for cloud-resolving boundary layer models to investigate the potential impact of ship emissions on cloud properties and their effects on the climate system. This may not only improve our general understanding of ship aerosol cloud interactions but also help in assessing the impact of Arctic based shipping activity.

Data Availability Statement

The data can be found at the Swedish National Data Service, an open access database, under <https://doi.org/10.5878/g1rx-zb70> (Santos et al., 2024).

References

Alanen, J., Isotalo, M., Kuittinen, N., Simonen, P., Martikainen, S., Kuuluvainen, H., et al. (2020). Physical characteristics of particle emissions from a medium speed ship engine fueled with natural gas and low-sulfur liquid fuels. *Environmental Science and Technology*, 54(9), 5376–5384. <https://doi.org/10.1021/acs.est.9b06460>

Alpert, P. A., Ciuraru, R., Rossignol, S., Passananti, M., Tinel, L., Perrier, S., et al. (2017). Fatty acid surfactant photochemistry results in new particle formation. *Scientific Reports*, 7(1), 12693. <https://doi.org/10.1038/s41598-017-12601-2>

Anastasopoulos, A. T., Sofowote, U. M., Hopke, P. K., Rouleau, M., Shin, T., Dheri, A., et al. (2021). Air quality in canadian port cities after regulation of low-sulphur marine fuel in the north american emissions control area. *Science of the Total Environment*, 791, 147949. <https://doi.org/10.1016/j.scitotenv.2021.147949>

Anderson, M., Salo, K., Hallquist, Å. M., & Fridell, E. (2015). Characterization of particles from a marine engine operating at low loads. *Atmospheric Environment*, 101(2015), 65–71. <https://doi.org/10.1016/j.atmosenv.2014.11.009>

Braun, A. (2005). Carbon speciation in airborne particulate matter with C (1s) NEXAFS spectroscopy. *Journal of Environmental Monitoring*, 7(11), 1059–1065. <https://doi.org/10.1039/b508910g>

Castarède, D., Brasseur, Z., Wu, Y., Kanji, Z. A., Hartmann, M., Ahonen, L., et al. (2023). Development and characterization of the portable ice nucleation chamber 2 (pincii). *Atmospheric Measurement Techniques*, 16(16), 3881–3899. <https://doi.org/10.5194/amt-16-3881-2023>

Corbett, J. J., Winebrake, J. J., Green, E. H., Kasibhatla, P., Eyring, V., & Lauer, A. (2007). Mortality from ship emissions: A global assessment. *Environmental Science and Technology*, 41(24), 8512–8518. <https://doi.org/10.1021/es071686z>

Corbin, J. C., Pieber, S. M., Czech, H., Zanatta, M., Jakobi, G., Massabò, D., et al. (2018). Brown and black carbon emitted by a marine engine operated on heavy fuel oil and distillate fuels: Optical properties, size distributions, and emission factors. *Journal of Geophysical Research: Atmospheres*, 123(11), 6175–6195. <https://doi.org/10.1029/2017JD027818>

Diamond, M. S. (2023). Detection of large-scale cloud microphysical changes within a major shipping corridor after implementation of the International Maritime Organization 2020 fuel sulfur regulations. *Atmospheric Chemistry and Physics*, 23(14), 8259–8269. <https://doi.org/10.5194/acp-23-8259-2023>

di Stasio, S., & Braun, A. (2006). Comparative NEXAFS study on soot obtained from an ethylene/air flame, a diesel engine, and graphite. *Energy and Fuels*, 20(1), 187–194. <https://doi.org/10.1021/ef058019g>

Eichler, P., Müller, M., Rohmann, C., Stengel, B., Orasche, J., Zimmermann, R., & Wisthaler, A. (2017). Lubricating oil as a major constituent of ship exhaust particles. *Environmental Science and Technology Letters*, 4(2), 54–58. <https://doi.org/10.1021/acs.estlett.6b00488>

Fauré, N., Chen, J., Artiglia, L., Ammann, M., Bartels-Rausch, T., Li, J., et al. (2023). Unexpected behavior of chloride and sulfate ions upon surface solvation of Martian salt analogue. *ACS Earth and Space Chemistry*, 7(2), 350–359. <https://doi.org/10.1021/acsearthspacechem.2c00204>

Flagiello, D., Di Natale, F., Lancia, A., & Salo, K. (2021). Effect of seawater Alkalinity on the performances of a marine diesel engine desulfurization scrubber. *Chemical Engineering Transactions*, 86, 505–510. <https://doi.org/10.3303/CET2186085>

Fridell, E., & Salo, K. (2016). Measurements of abatement of particles and exhaust gases in a marine gas scrubber. *Proceedings of the Institution of Mechanical Engineers - Part M: Journal of Engineering for the Maritime Environment*, 230(1), 154–162. <https://doi.org/10.1177/1475090214543716>

Fridell, E., Steen, E., & Peterson, K. (2008). Primary particles in ship emissions. *Atmospheric Environment*, 42(6), 1160–1168. <https://doi.org/10.1016/j.atmosenv.2007.10.042>

Friedman, B., Kulkarni, G., Beránek, J., Zelenyuk, A., Thornton, J. A., & Cziczo, D. J. (2011). Ice nucleation and droplet formation by bare and coated soot particles. *Journal of Geophysical Research*, 116(17), 1–11. <https://doi.org/10.1029/2011JD015999>

Gao, K., & Kanji, Z. A. (2022). Impacts of cloud-processing on ice nucleation of soot particles internally mixed with sulfate and organics. *Journal of Geophysical Research: Atmospheres*, 127(22), e2022JD037146. <https://doi.org/10.1029/2022JD037146>

Gryspeerd, E., Smith, T. W. P., O’Keeffe, E., Christensen, M. W., & Goldsworth, F. W. (2019). The impact of ship emission controls recorded by cloud properties. *Geophysical Research Letters*, 46(21), 12547–12555. <https://doi.org/10.1029/2019GL084700>

Acknowledgments

This research was funded by the Swedish Research Councils FORMAS (2017-00564) and VR (2020-03497 & 2021-04042). We acknowledge MAX IV Laboratory for time on Beamline SoftiMAX under Proposal 20220979. Research conducted at MAX IV, a Swedish national user facility, is supported by the Swedish Research council under contract 2018-07152, the Swedish Governmental Agency for Innovation Systems under contract 2018-04969, and Formas under contract 2019-02496. The sulfur STXM/NEXAFS result was obtained at the BL4U of UVSOR Synchrotron Facility, Institute for Molecular Science (IMS program 22IMS6638). EST and LS thank the Swedish Strategic Research Area MERGE for support. X.K. acknowledges the support from the Swedish Foundation for International Cooperation in Research and Higher Education (CH2019-8361). We would like to thank Anders Mattsson and Timothy Benham from Chalmers University for great support and assistance during the measurement campaign. We would like to thank Birgitta Svenningsson from Lund University’s aerosol physics group for use of the CCNC. Oliver Hoedt, a visiting Erasmus+ student, contributed greatly to the experimental measurements.

- Henning, S., Ziese, M., Kiselev, A., Saathoff, H., Möhler, O., Mentel, T. F., et al. (2012). Hygroscopic growth and droplet activation of soot particles: Uncoated, succinic or sulfuric acid coated. *Atmospheric Chemistry and Physics*, 12(10), 4525–4537. <https://doi.org/10.5194/acp-12-4525-2012>
- Hinds, W. C. (1999). *Aerosol technology: Properties, behavior, and measurement of airborne particles* (2nd ed.). Wiley.
- Hitchcock group homepage. (2023). Retrieved from <http://unicorn.mcmaster.ca/axis/aXis2000-IDLVM.html>. accessed on 2023 23 07.
- IMO. (2008). Revised marpol Annex VI - amendments to the annex of the protocol of 1997 to amend the international convention for the prevention of pollution from SHIPS, 1973, as modified by the protocol of 1978 relating thereto. *MEPC*, 176(58), 101.
- IMO. (2021a). 2021 guidelines for exhaust gas cleaning systems. *Resolution MEPC*, 340(77).
- IMO. (2021b). Prohibition on the use and carriage for use as fuel of heavy fuel oil by ships in Arctic waters. *Resolution MEPC*, 329(76).
- IPCC. (2021). *Climate change 2021: The physical science basis. contribution of working group I to the sixth assessment report of the intergovernmental panel on climate change*. Cambridge University Press. In Press [Book]. <https://doi.org/10.1017/9781009157896>
- Järvinen, A., Lehtoranta, K., Aakko-Saksa, P., Karppanen, M., Murtonen, T., Martikainen, J., et al. (2023). Performance of a wet electrostatic precipitator in marine applications. *Journal of Marine Science and Engineering*, 11(2), 393. <https://doi.org/10.3390/jmse11020393>
- Jeong, S., Bendl, J., Saraji-Bozorgzad, M., Käfer, U., Etzien, U., Schade, J., et al. (2023). Aerosol emissions from a marine diesel engine running on different fuels and effects of exhaust gas cleaning measures. *Environmental Pollution*, 316, 120526. <https://doi.org/10.1016/j.envpol.2022.120526>
- Kasper, A., Aufdenblatten, S., Forss, A., Mohr, M., & Burtscher, H. (2007). Particulate emissions from a low-speed marine diesel engine. *Aerosol Science and Technology*, 41(1), 24–32. <https://doi.org/10.1080/02786820601055392>
- Khalizov, A. F., Zhang, R., Zhang, D., Xue, H., Pagels, J., & McMurry, P. H. (2009). Formation of highly hygroscopic soot aerosols upon internal mixing with sulfuric acid vapor. *Journal of Geophysical Research*, 114(5), 1–15. <https://doi.org/10.1029/2008JD010595>
- Kong, X., Gladich, I., Fauré, N., Thomson, E. S., Chen, J., Artiglia, L., et al. (2023). Adsorbed water promotes chemically active environments on the surface of sodium chloride. *Journal of Physical Chemistry Letters*, 14(26), 6151–6156. <https://doi.org/10.1021/acs.jpclett.3c00980>
- Kong, X., Priestley, M., Pei, X., Zhu, Y., Wu, Z., Hu, M., & Hallquist, M. (2023). *Chemical mapping of potassium-containing particles from residential biomass burning and in ambient air*. In (p. 020003). <https://doi.org/10.1063/5.0168163>
- Koop, T., Luo, B., Tsias, A., & Peter, T. (2000). Water activity as the determinant for homogeneous ice nucleation in aqueous solutions. *Nature*, 406(6796), 611–614. <https://doi.org/10.1038/35020537>
- Korhonen, K., Kristensen, T. B., Falk, J., Malmborg, V. B., Eriksson, A., Gren, L., et al. (2022). Particle emissions from a modern heavy-duty diesel engine as ice nuclei in immersion freezing mode: A laboratory study on fossil and renewable fuels. *Atmospheric Chemistry and Physics*, 22(3), 1615–1631. <https://doi.org/10.5194/acp-22-1615-2022>
- Kristensen, T. B., Falk, J., Lindgren, R., Andersen, C., Malmborg, V. B., Eriksson, A. C., et al. (2021). Properties and emission factors of cloud condensation nuclei from biomass cookstoves – Observations of a strong dependency on potassium content in the fuel. *Atmospheric Chemistry and Physics*, 21(10), 8023–8044. <https://doi.org/10.5194/acp-21-8023-2021>
- Kristineberg center homepage. (2024). Retrieved from <https://www.gu.se/en/kristineberg/infrastructure-and-services> (accessed on 2024-01-17)
- Lance, S., Medina, J., Smith, J., & Nenes, A. (2006). Mapping the operation of the DMT continuous flow CCN counter. *Aerosol Science and Technology*, 40(4), 242–254. <https://doi.org/10.1080/02786820500543290>
- Lehtoranta, K., Aakko-Saksa, P., Murtonen, T., Vesala, H., Ntziachristos, L., Rönkkö, T., et al. (2019). Particulate mass and nonvolatile particle number emissions from marine engines using low-sulfur fuels, natural gas, or scrubbers. *Environmental Science and Technology*, 53(6), 3315–3322. <https://doi.org/10.1021/acs.est.8b05555>
- Leinweber, P., Kruse, J., Walley, F. L., Gillespie, A., Eckhardt, K.-U., Blyth, R. I. R., & Regier, T. (2007). Nitrogen K -edge XANES – An overview of reference compounds used to identify ‘unknown’ organic nitrogen in environmental samples. *Journal of Synchrotron Radiation*, 14(6), 500–511. <https://doi.org/10.1107/S0909049507042513>
- Lieke, K. I., Rosenørn, T., Pedersen, J., Larsson, D., Kling, J., Fuglsang, K., & Bilde, M. (2013). Micro- and nanostructural characteristics of particles before and after an exhaust gas recirculation system scrubber. *Aerosol Science and Technology*, 47(9), 1038–1046. <https://doi.org/10.1080/02786826.2013.813012>
- Liu, H., Fu, M., Jin, X., Shang, Y., Shindell, D., Faluvegi, G., et al. (2016). Health and climate impacts of ocean-going vessels in East Asia. *Nature Climate Change*, 6(11), 1037–1041. <https://doi.org/10.1038/nclimate3083>
- Lunde Hermansson, A., Hassellöv, I.-M., Moldanová, J., & Ytreberg, E. (2021). Comparing emissions of polyaromatic hydrocarbons and metals from marine fuels and scrubbers. *Transportation Research Part D: Transport and Environment*, 97, 102912. <https://doi.org/10.1016/j.trd.2021.102912>
- Mahrt, F., Alpert, P. A., Dou, J., Grönquist, P., Arroyo, P. C., Ammann, M., et al. (2020). Aging induced changes in ice nucleation activity of combustion aerosol as determined by near edge X-ray absorption fine structure (NEXAFS) spectroscopy. *Environmental Sciences: Processes and Impacts*, 22(4), 895–907. <https://doi.org/10.1039/C9EM00525K>
- Mahrt, F., Kilchhofer, K., Marcolli, C., Grönquist, P., David, R. O., Rösch, M., et al. (2020). The Impact of cloud processing on the ice nucleation abilities of soot particles at cirrus temperatures. *Journal of Geophysical Research: Atmospheres*, 125(3), 1–23. <https://doi.org/10.1029/2019JD030922>
- Manshausen, P., Watson-Parris, D., Christensen, M. W., Jalkanen, J.-p., & Stier, P. (2022). Invisible ship tracks show large cloud sensitivity to aerosol. *Nature*, 610(7930), 101–106. <https://doi.org/10.1038/s41586-022-05122-0>
- Moffet, R. C., Tivanski, A. V., & Gilles, M. K. (2010). In R. Signorell & J. Reid (Eds.), *Scanning transmission X-ray microscopy: Applications in atmospheric aerosol research*. Taylor and Francis Books Inc.
- Möhler, O., Büttner, S., Linke, C., Schnaiter, M., Saathoff, H., Stetzer, O., et al. (2005). Effect of sulfuric acid coating on heterogeneous ice nucleation by soot aerosol particles. *Journal of Geophysical Research: Atmosphere*, 110(11), 1–12. <https://doi.org/10.1029/2004JD005169>
- Moldanová, J., Fridell, E., Popovicheva, O., Demirdjian, B., Tishkova, V., Faccinnetto, A., & Focsa, C. (2009). Characterisation of particulate matter and gaseous emissions from a large ship diesel engine. *Atmospheric Environment*, 43(16), 2632–2641. <https://doi.org/10.1016/j.atmosenv.2009.02.008>
- Moldanová, J., Fridell, E., Winnes, H., Holmin-Fridell, S., Boman, J., Jedynska, A., et al. (2013). Physical and chemical characterisation of PM emissions from two ships operating in European Emission Control Areas. *Atmospheric Measurement Techniques*, 6(12), 3577–3596. <https://doi.org/10.5194/amt-6-3577-2013>
- Momenimovahed, A., Gagné, S., Gajdosechova, Z., Corbin, J. C., Smallwood, G. J., Mester, Z., et al. (2021). Effective density and metals content of particle emissions generated by a diesel engine operating under different marine fuels. *Journal of Aerosol Science*, 151, 105651. <https://doi.org/10.1016/j.jaerosci.2020.105651>
- Moore, R. H., & Nenes, A. (2009). Scanning flow ccn analysis—A method for fast measurements of ccn spectra. *Aerosol Science and Technology*, 43(12), 1192–1207. <https://doi.org/10.1080/02786820903289780>

- Olfert, J., & Rogak, S. (2019). Universal relations between soot effective density and primary particle size for common combustion sources. *Aerosol Science and Technology*, 53(5), 485–492. <https://doi.org/10.1080/02786826.2019.1577949>
- Olfert, J., Symonds, J., & Collings, N. (2007). The effective density and fractal dimension of particles emitted from a light-duty diesel vehicle with a diesel oxidation catalyst. *Journal of Aerosol Science*, 38(1), 69–82. <https://doi.org/10.1016/j.jaerosci.2006.10.002>
- Ouf, F.-X., Bourrous, S., Fauvel, S., Kort, A., Lintis, L., Nuvoli, J., & Yon, J. (2019). True density of combustion emitted particles: A comparison of results highlighting the influence of the organic contents. *Journal of Aerosol Science*, 134, 1–13. <https://doi.org/10.1016/j.jaerosci.2019.04.007>
- Park, K., Cao, F., Kittelson, D. B., & McMurry, P. H. (2003). Relationship between particle mass and mobility for diesel exhaust particles. *Environmental Science and Technology*, 37(3), 577–583. <https://doi.org/10.1021/es025960v>
- Peters, G. P., Nilsson, T. B., Lindholt, L., Eide, M. S., Glomsrød, S., Eide, L. I., & Fuglestad, J. S. (2011). Future emissions from shipping and petroleum activities in the Arctic. *Atmospheric Chemistry and Physics*, 11(11), 5305–5320. <https://doi.org/10.5194/acp-11-5305-2011>
- Petters, M. D., & Kreidenweis, S. M. (2007). A single parameter representation of hygroscopic growth and cloud condensation nucleus activity. *Atmospheric Chemistry and Physics*, 7(8), 1961–1971. <https://doi.org/10.5194/acp-7-1961-2007>
- Popovicheva, O., Kireeva, E., Shonija, N., Zubareva, N., Persiantseva, N., Tishkova, V., et al. (2009). Ship particulate pollutants: Characterization in terms of environmental implication. *Journal of Environmental Monitoring*, 11(11), 2077–2086. <https://doi.org/10.1039/b908180a>
- Priestley, M., Pei, X., Ohigashi, T., Yuzawa, H., Pettersson, J. B. C., Pathak, R. K., et al. (2023). Transformation of morphological and chemical properties by coating materials on soot. *AIP Conference Proceedings*, 2990(1), 020004. <https://doi.org/10.1063/5.0168166>
- Rissler, J., Messing, M. E., Malik, A. I., Nilsson, P. T., Nordin, E. Z., Bohgard, M., et al. (2013). Effective density characterization of soot agglomerates from various sources and comparison to aggregation theory. *Aerosol Science and Technology*, 47(7), 792–805. <https://doi.org/10.1080/02786826.2013.791381>
- Roberts, G. C., & Nenes, A. (2005). A continuous-flow streamwise thermal-gradient CCN chamber for atmospheric measurements. *Aerosol Science and Technology*, 39(3), 206–221. <https://doi.org/10.1080/027868290913988>
- Santos, L. F. E. d., Salo, K., Kong, X., Hartmann, M., Sjöblom, J., & Thomson, E. S. (2024). Marine fuel regulations and engine emissions: Impacts on physicochemical properties, cloud activity and emission factors [Dataset]. *Atmospheric Sciences* <https://doi.org/10.5878/g1rx-zb70>
- Santos, L. F. E. d., Salo, K., Kong, X., Noda, J., Kristensen, T. B., Ohigashi, T., & Thomson, E. S. (2023). Changes in CCN activity of ship exhaust particles induced by fuel sulfur content reduction and wet scrubbing. *Environmental Sciences: Atmosphere*, 3(1), 182–195. <https://doi.org/10.1039/D2EA00081D>
- Santos, L. F. E. d., Salo, K., & Thomson, E. S. (2022). Quantification and physical analysis of nanoparticle emissions from a marine engine using different fuels and a laboratory wet scrubber. *Environmental Sciences: Processes and Impacts*, 24(10), 1769–1781. <https://doi.org/10.1039/D2EM00054G>
- Sarret, G., Connan, J., Kasrai, M., Bancroft, G. M., Charrié-Duhaut, A., Lemoine, S., et al. (1999). Chemical forms of sulfur in geological and archeological asphaltene from Middle East, France, and Spain determined by sulfur K- and L-edge X-ray absorption near-edge structure spectroscopy. *Geochimica et Cosmochimica Acta*, 63(22), 3767–3779. [https://doi.org/10.1016/S0016-7037\(99\)00205-7](https://doi.org/10.1016/S0016-7037(99)00205-7)
- Seppälä, S. D., Kuula, J., Hyvärinen, A.-P., Saarikoski, S., Rönkkö, T., Keskinen, J., et al. (2021). Effects of marine fuel sulfur restrictions on particle number concentrations and size distributions in ship plumes in the Baltic Sea. *Atmospheric Chemistry and Physics*, 21(4), 3215–3234. <https://doi.org/10.5194/acp-21-3215-2021>
- Sippula, O., Stengel, B., Sklorz, M., Streibel, T., Rabe, R., Orasche, J., et al. (2014). Particle emissions from a marine engine: Chemical composition and aromatic emission profiles under various operating conditions. *Environmental Science and Technology*, 48(19), 11721–11729. <https://doi.org/10.1021/es502484z>
- Tavakoli, F., & Olfert, J. S. (2014). Determination of particle mass, effective density, mass-mobility exponent, and dynamic shape factor using an aerodynamic aerosol classifier and a differential mobility analyzer in tandem. *Journal of Aerosol Science*, 75, 35–42. <https://doi.org/10.1016/j.jaerosci.2014.04.010>
- Tivanski, A. V., Hopkins, R. J., Tyliczcak, T., & Gilles, M. K. (2007). Oxygenated interface on biomass burn tar balls determined by single particle scanning transmission X-ray microscopy. *The Journal of Physical Chemistry A*, 111(25), 5448–5458. <https://doi.org/10.1021/jp070155u>
- Trivanovic, U., Corbin, J. C., Baldelli, A., Peng, W., Yang, J., Kirchen, P., et al. (2019). Size and morphology of soot produced by a dual-fuel marine engine. *Journal of Aerosol Science*, 138, 105448. <https://doi.org/10.1016/j.jaerosci.2019.105448>
- Watson-Parris, D., Christensen, M. W., Laurensen, A., Clewley, D., Gryspeerd, E., & Stier, P. (2022). Shipping regulations lead to large reduction in cloud perturbations. *Proceedings of the National Academy of Sciences*, 119(41). <https://doi.org/10.1073/pnas.2206885119>
- Weeraratna, C., Kostko, O., & Ahmed, M. (2022). An investigation of aqueous ammonium nitrate aerosols with soft X-ray spectroscopy. *Molecular Physics*, 120(1–2), e1983058. <https://doi.org/10.1080/00268976.2021.1983058>
- Winnes, H., Fridell, E., & Moldanová, J. (2020). Effects of marine exhaust gas scrubbers on gas and particle emissions. *Journal of Marine Science and Engineering*, 8(4), 299. <https://doi.org/10.3390/jmse8040299>
- Wittbom, C., Eriksson, A. C., Rissler, J., Carlsson, J. E., Roldin, P., Nordin, E. Z., et al. (2014). Cloud droplet activity changes of soot aerosol upon smog chamber ageing. *Atmospheric Chemistry and Physics*, 14(18), 9831–9854. <https://doi.org/10.5194/acp-14-9831-2014>
- Wu, Z., Zhang, Y., He, J., Chen, H., Huang, X., Wang, Y., et al. (2020). Dramatic increase in reactive volatile organic compound (VOC) emissions from ships at berth after implementing the fuel switch policy in the Pearl River Delta Emission Control Area. *Atmospheric Chemistry and Physics*, 20(4), 1887–1900. <https://doi.org/10.5194/acp-20-1887-2020>
- Yang, J., Tang, T., Jiang, Y., Karavalakis, G., Durbin, T. D., Wayne Miller, J., et al. (2021). Controlling emissions from an ocean-going container vessel with a wet scrubber system. *Fuel*, 304, 121323. <https://doi.org/10.1016/j.fuel.2021.121323>
- Ytreberg, E., Hansson, K., Hermansson, A. L., Parsmo, R., Lagerström, M., Jalkanen, J.-P., & Hassellöv, I.-M. (2022). Metal and PAH loads from ships and boats, relative other sources, in the Baltic Sea. *Marine Pollution Bulletin*, 182, 113904. <https://doi.org/10.1016/j.marpolbul.2022.113904>
- Yu, C., Pasternak, D., Lee, J., Yang, M., Bell, T., Bower, K., et al. (2020). Characterizing the particle composition and cloud condensation nuclei from shipping emission in western Europe. *Environmental Science and Technology*, 54(24), 15604–15612. <https://doi.org/10.1021/acs.est.0c04039>
- Yu, C., Pasternak, D., Lee, J., Yang, M., Bell, T., Bower, K., et al. (2023). Correction to “characterizing the particle composition and cloud condensation nuclei from shipping emission in western Europe”. *Environmental Science and Technology*, 57(20), 7888–7889. <https://doi.org/10.1021/acs.est.3c03005>
- Yuan, T., Song, H., Wood, R., Wang, C., Oreopoulos, L., Platnick, S. E., et al. (2022). Global reduction in ship-tracks from sulfur regulations for shipping fuel. *Science Advances*, 8(29), 1–9. <https://doi.org/10.1126/sciadv.abn7988>

- Zelenay, V., Ammann, M., Křepelová, A., Birrer, M., Tzvetkov, G., Vernooij, M. G., et al. (2011). Direct observation of water uptake and release in individual submicrometer sized ammonium sulfate and ammonium sulfate/adipic acid particles using X-ray microspectroscopy. *Journal of Aerosol Science*, *42*(1), 38–51. <https://doi.org/10.1016/j.jaerosci.2010.11.001>
- Zetterdahl, M., Salo, K., Fridell, E., & Sjöblom, J. (2017). Impact of aromatic concentration in marine fuels on particle emissions. *Journal of Marine Science and Application*, *16*(3), 352–361. <https://doi.org/10.1007/s11804-017-1417-7>
- Zhai, J., Yu, G., Zhang, J., Shi, S., Yuan, Y., Jiang, S., et al. (2023). Impact of ship emissions on air quality in the Greater Bay Area in China under the latest global marine fuel regulation. *Environmental Science and Technology*, *57*(33), 12341–12350. <https://doi.org/10.1021/acs.est.3c03950>
- Zhou, J., Zhou, S., & Zhu, Y. (2017). Characterization of particle and gaseous emissions from marine diesel engines with different fuels and impact of after-treatment technology. *Energies*, *10*(8), 1110. <https://doi.org/10.3390/en10081110>